AN INTRODUCTORY THEORETICAL ANALYSIS OF PLANAR COMPLIANT COUPLINGS

By

THOMAS M. PIGOSKI II

A THESIS PRESENTED TO THE GRADUATE SCHOOL
OF THE UNIVERSITY OF FLORIDA IN PARTIAL FULFILLMENT
OF THE REQUIREMENTS FOR THE DEGREE OF
MASTER OF SCIENCE

UNIVERSITY OF FLORIDA

1993

TABLE OF CONTENTS

LIST OF FIGURES

Abstract of Thesis Presented to the Graduate School
of the University of Florida in Partial Fulfillment of the
Requirements for the Degree of Master of Science

AN INTRODUCTORY THEORETICAL ANALYSIS OF PLANAR COMPLIANT COUPLINGS

By

Thomas M. Pigoski II

December, 1993

Chairperson: Dr. Joseph Duffy
Major Department: Mechanical Engineering

The behavior of two simple compliant couplings was analyzed with the intent of better understanding the force and position relationship for improved control.

A closed-form inverse analysis was performed on a planar two-spring coupling. The two springs were grounded to pivots at one end and attached to a common pivot at the other. A known force was applied to the common pivot of the system, and it was required to determine all of the assembly configurations. At the outset this appeared to be a relatively simple problem. However, this proved not to be the case. By variable elimination, a sixth degree polynomial in the resultant length of one spring was derived, and from this, six unique locations of the point of application of force were obtained. The results were verified numerically by performing a forward force analysis and displaying real solutions. It is clear there are a maximum of six mathematical assembly

configurations to obtain the desired force for such a spring system. Additionally, the applied force was incremented, and the motion of all six configurations was tracked. The behavior of this system exhibited signs of both negative stiffness and catastrophe.

The stiffness mapping for a planar three-spring coupling was analyzed using two different reference frames. The first was rigidly attached to the fixed body of the coupling, while the second is attached to the moving body of the coupling. It was found that, in general, these matrices are asymmetric when the coupling is loaded, and that one is the transpose of the other. These new mappings are essential for the control of the coupling as it moves away from the its unloaded position. Additionally, a third frame of reference which produces a symmetric mapping is examined and found to be identical to the Hessian obtained from the second differentials of the elastic potential energy of the system. However, this symmetric mapping is not useful for control purposes and is only included to show that such a frame can be realized. Finally, static force loci for each of the reference frames are drawn to support the notion of frame-of-reference dependency.

CHAPTER 1
TWO PLANAR COMPLIANT COUPLINGS

Compliant parallel mechanisms have, for a long time, played a significant role in areas of force application such as mounting and suspension systems. However, recent advances in the field of simultaneous force and position control of a robotic end-effector using compliant couplings have brought about a renewed interest in their behavior. These mechanisms can be modeled as generalized spatial springs consisting of multiple linear springs acting in parallel to connect two rigid bodies. In the proposed force-control application, a coupling would be introduced to connect a gripper\workpiece with the end link of a robotic manipulator. The purpose of this thesis is to examine the behavior of two simple planar compliant couplings: the planar two-spring coupling and the planar three-spring coupling.

1.1 The Planar Two-Spring Coupling

The first device analyzed was a planar two-spring coupling. The device shown in Figure 1.1 in equilibrium with the externally applied static forces Fx and Fy, consists of two simple translational springs acting in parallel, one grounded at pivot point A and the other grounded at pivot point B. The other ends of the springs are connected and pivoted at point P. Each of the springs can be thought of as acting in the prismatic joint of a revolute-prismatic-revolute serial chain. For this mechanism, it is assumed that the free lengths and

elasticity constants of the springs are known along with the distance between pivots A and B.

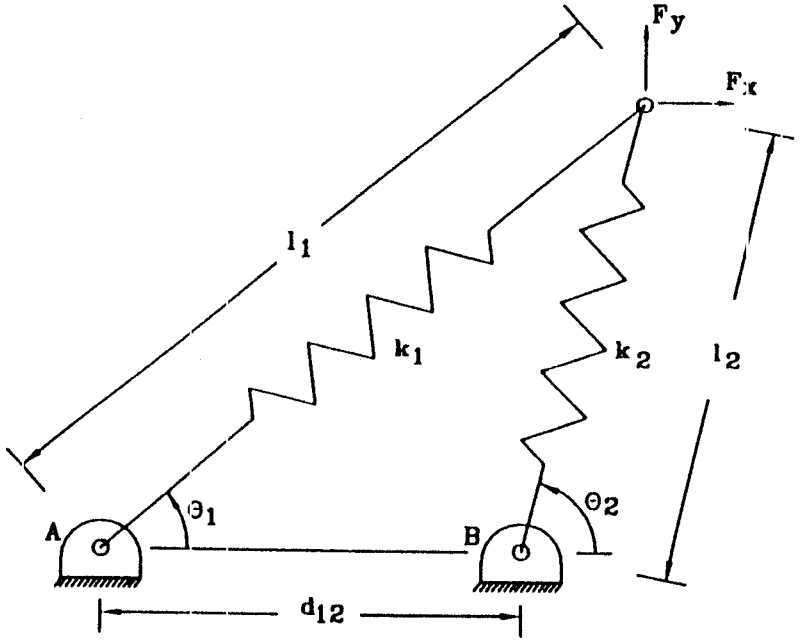

Figure 1.1 Planar Two-Spring Coupling

As far as this author is aware, very little work has been done on the closed-form inverse analysis of this device. Most of the literature has devoted itself to forward force analysis which is inherently simple(viz. the resulting force acting upon a common pivot is easily computed for a specified pivot location). Vanderrplaats[1] has investigated a nonlinear, iterative inverse analysis, whereby the displacement field of the structure under a given loading is found by minimizing the total potential energy of the system. Numerically this method produces a single solution to the problem. Also, Seireg[2] has used an algorithmic approximation to obtain a single geometric solution for systems under small loads and undergoing small displacements from the unloaded configuration.

Additional literature which is important concerns the instantaneous kinestatics of the planar two-parameter spring. Theoretical and experimental work by Griffis[3] has shown that instantaneous control of force and displacement could be achieved with this device through position control alone. A global stiffness mapping was developed which is dependent on the instantaneous geometry of the device and can be used to correlate a small change in the force applied by the mechanism into a corresponding relative motion. This mapping is global because it holds true when the spatial spring is displaced far from the unloaded configuration. Of significance for this analysis is the fact that Griffis[4] found this mapping essential in determining the stability of the mechanism in a given configuration. The development of this mapping is included in Chapter 2 of this thesis for the sake of completeness.

In Chapter 3, a closed-form inverse force analysis is performed on the planar two-spring coupling. A known force is applied to the common pivot of the system, and it was required to determine all of the assembly configurations. Additionally, the motion of the common pivot is analyzed as the applied force is changed along a spectrum. The appearance of negative spring lengths occurred in several examples, so a section on their significance is included.

1.2 The Planar Three-Spring Coupling

The second device analyzed is the planar three-parameter coupling. The coupling, shown in Figure 1.2 in equilibrium with an external static force \$, consists of two rigid bodies connected together via three translational springs acting in parallel. Again each of the springs can be considered as acting in the prismatic joint of a revolute-prismatic-revolute serial chain. Again, it is assumed

that the spring constants and free lengths of the springs are known. However, it is not assumed that the springs are at their respective free lengths, and hence, the coupling is assumed to be loaded which requires that an external static force be applied to the moving body to keep it in static equilibrium.

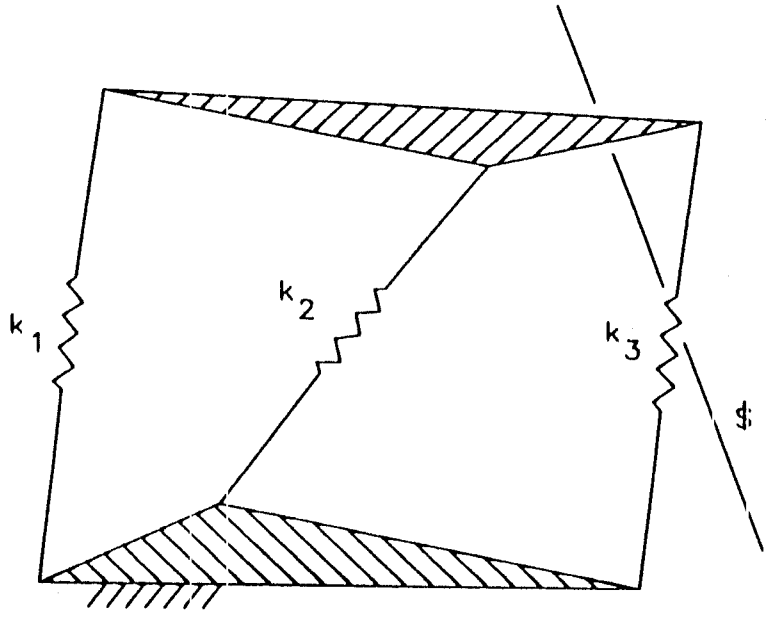

Figure 1.2 Planar Three-Spring Coupling

A new theory for the simultaneous control of force and displacement of a partially constrained end-effector has been proposed (see Griffis and Duffy[5], Griffis[3]). The spatial stiffness of a compliant coupling which connects two rigid bodies is used to map a small relative twist into a corresponding interactive wrench increment. This work can be considered an extension of the work done by Dimentberg[6], who derived a symmetrical stiffness mapping for an unloaded coupling. Several other authors have reported successful results using specialized

couplings dependent on the existence of a center of compliance. (See Salisbury[7], Mason[8], Raibert and Craig[9], Whitney[10], and Mason[11].) However, the impetus for this research was the appearance of asymmetrical stiffness mappings reported by Griffis and Duffy[5] and Griffis[3] which at the outset appeared to be incompatible with the previously reported symmetric mappings.

In Chapter 4 of this thesis the stiffness mapping for the planar three-parameter coupling is derived for three different reference frames. The first is rigidly attached to the fixed body of the coupling (see Griffis and Duffy[5]), while the second is rigidly attached to the moving body of the coupling. These mappings are essential for the control of the coupling as it moves away from the unloaded configuration since it is to these two frames which a force\torque sensor can be mounted to sense the actual static force applied to the moving body. The third reference frame was from a body that undergoes rectilinear motion with respect to the fixed body and is hinged to the moving body. This reference frame always produces a symmetric mapping. This mapping is identical to the Hessian obtained from the second differentials of the elastic potential energy function (see Lončarić[12]). Although yielding a simple symmetric mapping, this cannot be used in the control algorithm discussed above because no force\torque sensor can be mounted in this reference frame. Additionally, the static force line loci necessary to produce a specified relative motion between the moving and fixed bodies of the coupling are included to provide another example of the frame-of-reference dependency inherent in Chapter 4. For all three reference frames the force locus is different, but at any instant, all such loci are shown to share the same common tangent along which the current static force is applied to the moving body.

CHAPTER 2
KINESTATICS OF COMPLIANT COUPLINGS

This chapter contains a theoretical development of planar kinestatics which will be used in later chapters.

2.1 Generalized Line Coordinates

The two distinct points $\underline{r}_1(x_1,y_1)$ and $\underline{r}_2(x_2,y_2)$ determine the line \$ shown in Fig. 2.1. The line segment $\underline{S}$ joining the two points can be expressed in the form

$$\underline{S} = L\underline{i} + M\underline{j} \tag{2.1}$$

where

$$L = x_2 - x_1 \quad \text{and} \quad M = y_2 - y_1 \tag{2.2}$$

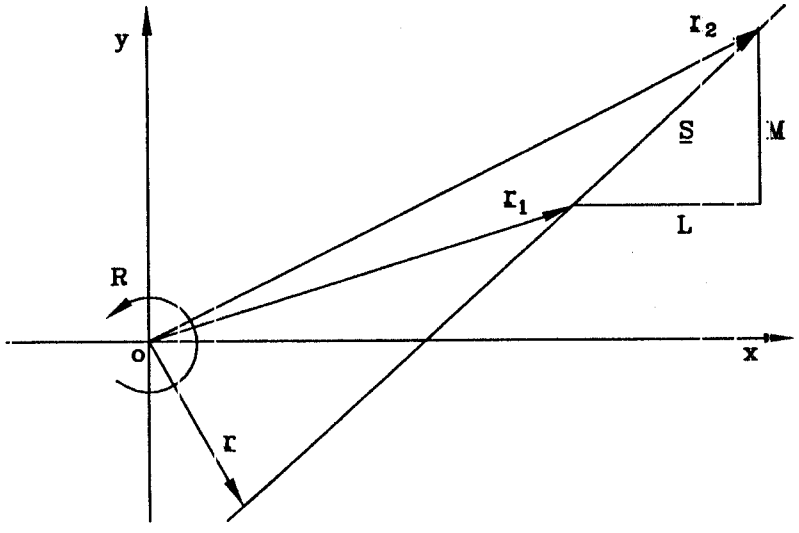

Figure 2.1 A Line in the xy Plane

are the direction ratios of the line segment. These direction ratios are related to the distance between the two points by the relation

$$L^2 + M^2 = |\underline{S}|^2. \tag{2.3}$$

The moment of the directed line segment about the origin is given by the the vector product $\underline{r}x\underline{S}$ where $\underline{r}$ is any vector drawn from the origin to any point contained on the unlimited line joining $\underline{r}_1$ and $\underline{r}_2$. Since the vector $(\underline{r}-\underline{r}_1)$ will be parallel to $\underline{S}$, the equation of a line can be written as

$$(\underline{r}-\underline{r}_1) \times \underline{S} = 0. \tag{2.4}$$

This equation can be expressed in the form

$$\underline{r} \times \underline{S} = \underline{S}_O , \tag{2.5}$$

where

$$\underline{S}_O = \underline{r}_1 \times \underline{S} , \tag{2.6}$$

is the moment of the line about the origin represented by a vector $R\underline{k}$ perpendicular to the plane. The vector $[\underline{S};\underline{S}_O]^T$ can also be represented by the ordered triple of real numbers (L,M;R) which are the homogeneous coordinates of the unlimited line and must satisfy the orthogonality condition

$$\underline{S} \cdot \underline{S}_O = 0. \tag{2.7}$$

They were first established by Plücker[13,14] and for this reason are called the Plücker line coordinates. They are homogeneous since the coordinates $(\lambda\underline{S};\ \lambda\underline{S}_O)$ where λ is a nonzero scalar determine the same line.

The directed line segment described above can be considered as equivalent to a force applied to a rigid body. Plücker defined a force together with its corresponding moment vector about the origin as a wrench. A wrench on a line will be represented as a general "ray" that is assigned the vector $\hat{w} = [\underline{f};\underline{m}_O]^T$, where $\underline{f}$ is the force vector in the direction of the wrench and $\underline{m}_O$ is the moment

vector referenced to the origin. Ray coordinates for lines (direction vector first) are based on Plücker's definition of a ray as a line formed from the joining of two points. Rays are usually assigned lower case labels. Plücker defined a rotation about a line as a twist. A twist on a line can be represented as a general "axis" that is assigned the vector $\hat{D} = [\delta\underline{\theta};\underline{S}]^T$, where $\delta\underline{\theta}$ is the magnitude of the rotation and $\underline{S}$ is the direction of the line of rotation. Axis coordinates for lines (direction vector second) are based on Plücker's definition of an axis as a line formed by the meet of two planes. Axis coordinates are usually assigned upper case labels. Transformations which map an axis to a ray (or a ray to an axis) are defined as correlation, while transformations which map an axis to an axis (or a ray to a ray) are called collineations.

2.2 The Mutual Moment of a Pair of Lines

Figure 2.2 illustrates a line $\$_i$ in the xy plane with ray coordinates

$$\hat{s}_i = \begin{bmatrix} c_i \\ s_i \\ r_i + r_i' \end{bmatrix} \tag{2.8}$$

where c_i and s_i are respectively the $\cos(\theta_i)$ and $\sin(\theta_i)$. Consider now that there is a second line \$, drawn through the point G perpendicular to the xy plane with axis coordinates

$$\hat{S} = \begin{bmatrix} y_G \\ -x_G \\ 1 \end{bmatrix}. \tag{2.9}$$

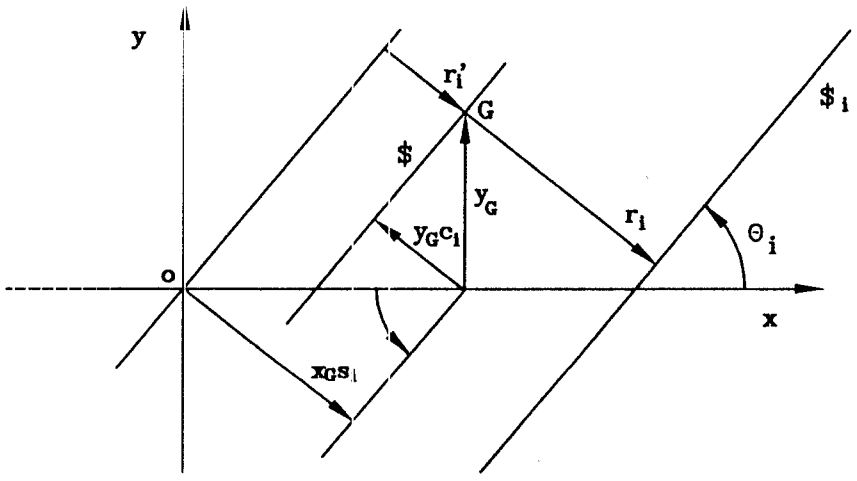

Figure 2.2 The Mutual Moment of a Pair of Lines

The mutual moment is defined as $\hat{s}_i^T \hat{S}$ $(= \hat{S}^T \hat{s}_i)$. From (2.8) and (2.9),

$$\hat{s}_i^T \hat{S} = [c_i, s_i; r_i+r_i'] \begin{bmatrix} y_G \\ -x_G \\ 1 \end{bmatrix}$$

$$= r_i+r_i'-(x_G s_i - y_G c_i). \tag{2.10}$$

From Fig. 2.2, $(x_G s_i - y_G c_i) = r_i'$ and therefore

$$\hat{s}_i^T \hat{S} = r_i \, . \tag{2.11}$$

The mutual moment for these pair of lines which are themselves mutually perpendicular is clearly their common perpendicular distance r_i, and it is an invariant.

2.3 The Stiffness Mapping Matrix

The spatial stiffness of a compliant coupling which connects two rigid bodies can be used to map a small relative twist into a corresponding interactive wrench increment. In its general form, the mapping is

$$\delta\hat{w} = [K]\ \delta\hat{D}, \tag{2.12}$$

where $\delta\hat{w}$ are the ray coordinates of a wrench increment, $\delta\hat{D}$ are the axis coordinates of an infinitesimal twist, and [K] is the stiffness mapping defendant upon the geometrical and material stiffness properties of the coupling.

The stiffness mapping of a planar two-parameter coupling is re-derived following Griffis[3]:

In Figure 2.3, an external force $\underline{f} = F_x\ \underline{i} + F_y\ \underline{j}$ is applied to the system at point P. The force is in static equilibrium with the forces in the springs , and the system is to remain in static equilibrium as the point P displaces.

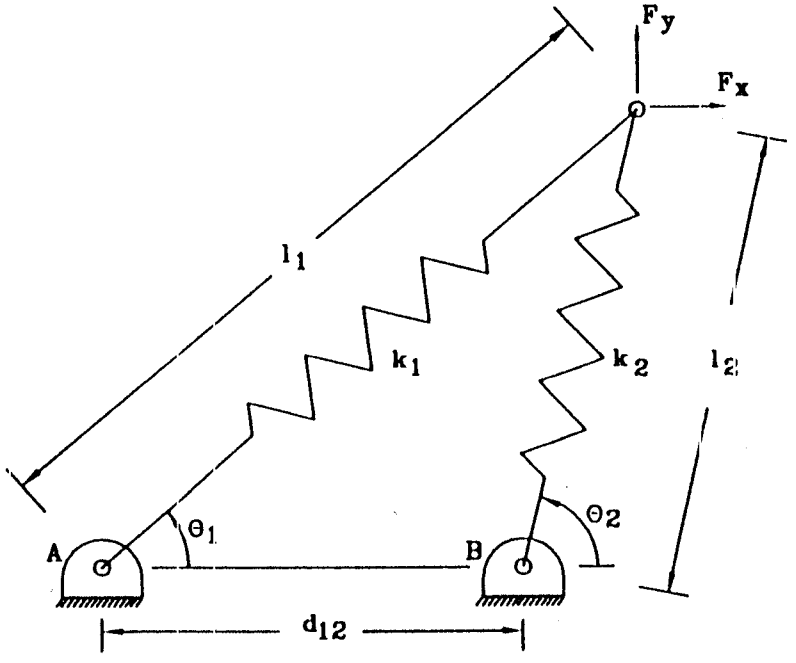

Figure 2.3 Planar Two-Spring Coupling

It is necessary to determine the mapping of stiffness

$$\delta \underline{f} = [K]\, \delta \underline{d} \tag{2.13}$$

where $\delta \underline{f} = \delta F_x\, \underline{i} + \delta F_y\, \underline{j}$ i a small increment in $\underline{f}$ that is related via [K] to a small displacement $\delta \underline{d} = \delta x\, \underline{i} + \delta y\, \underline{j}$ of point P. Based on the locations of points A, B, and P, the lengths l_1 and l_2 and the angles θ_1 and θ_2 can be computed.

In order to derive the mapping of stiffness (2.13) it is necessary to express the external static force applied to the pivot as a resultant of the forces in the springs:

$$\begin{bmatrix} F_x \\ F_y \end{bmatrix} = \begin{bmatrix} c_1 & c_2 \\ s_1 & s_2 \end{bmatrix} \begin{bmatrix} k_1(l_1 - l_{o1}) \\ k_2(l_2 - l_{o2}) \end{bmatrix}, \tag{2.14}$$

where $c_i = \cos(\theta_i)$ and $s_i = \sin(\theta_i)$, and where k_i and $(l_i - l_{oi})$ are respectively the positive non-zero spring constant and the difference between the current and free lengths of the i^{th} spring.

To obtain the mapping it is necessary to differentiate (2.14). A complete differential gives

$$\begin{bmatrix} \delta F_x \\ \delta F_y \end{bmatrix} = \begin{bmatrix} c_1 & s_2 \\ s_1 & s_2 \end{bmatrix} \begin{bmatrix} k_1 & \delta l_1 \\ k_2 & \delta l_2 \end{bmatrix} + \begin{bmatrix} -s_1 & -s_2 \\ c_1 & c_2 \end{bmatrix} \begin{bmatrix} k_1(l_1 - l_{o1})\ \delta\theta_1 \\ k_2(l_2 - l_{o2})\ \delta\theta_2 \end{bmatrix} \tag{2.15}$$

where δF_x and δF_y are the change in force applied to the point P, δl_1 and δl_2 are the change in length of the springs, and $\delta\theta_1$ and $\delta\theta_2$ are the change in the angles θ_1 and θ_2. An equivalent form of (2.15) is

$$\begin{bmatrix} \delta F_x \\ \delta F_y \end{bmatrix} = \begin{bmatrix} c_1 & c_2 \\ s_1 & s_2 \end{bmatrix} \begin{bmatrix} k_1 & \delta l_1 \\ k_2 & \delta l_2 \end{bmatrix} + \begin{bmatrix} -s_1 & -s_2 \\ c_1 & c_2 \end{bmatrix} \begin{bmatrix} k_1(1 - \rho_1)\ l_1\delta\theta_1 \\ k_2(1 - \rho_2)\ l_2\delta\theta_2 \end{bmatrix} \tag{2.16}$$

where the parameters, $\rho_i = l_{oi}/l_i$ have been introduced. Now, in order to obtain the mapping (2.13), it remains only to make substitutions of δx and δy for δl_i and $l_i \delta\theta_i$. Rearranging (2.16) into the form

$$\begin{bmatrix} \delta F_x \\ \delta F_y \end{bmatrix} = \begin{bmatrix} c_1 & c_2 \\ s_1 & s_2 \end{bmatrix} \begin{bmatrix} k_1 & 0 \\ 0 & k_2 \end{bmatrix} \begin{bmatrix} \delta l_1 \\ \delta l_2 \end{bmatrix}$$
$$+ \begin{bmatrix} -s_1 & -s_2 \\ c_1 & c_2 \end{bmatrix} \begin{bmatrix} k_1(1-\rho_i) & 0 \\ 0 & k_2(1-\rho_2) \end{bmatrix} \begin{bmatrix} l_1 \delta\theta_1 \\ l_2 \delta\theta_2 \end{bmatrix} \tag{2.17}$$

which will facilitate the substitutions necessary.

Figure 2.4 illustrates the motion of the i^{th} spring of the coupling as it displaces $\delta \underline{d}$. This displacement can be decomposed into two components: an infinitesimal displacement δl_i along the direction of the spring, $\underline{s}_i = c_1 \underline{i} + s_i \underline{j}$, together with an infinitesimal displacement $l_i \delta\theta_i$ that is tangent to circle of

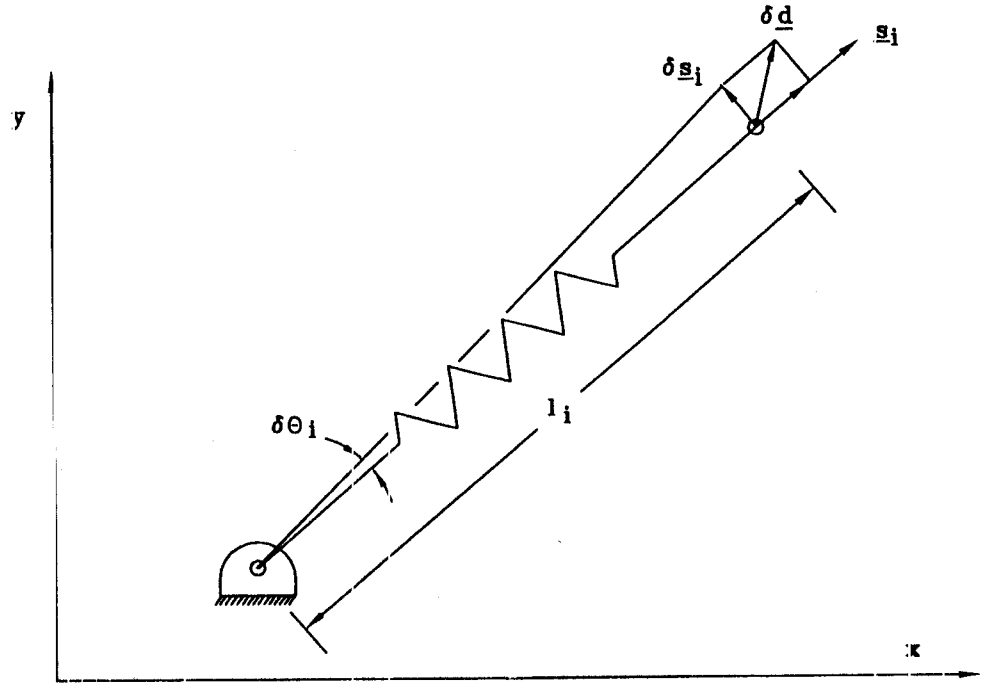

Figure 2.4: Motion of an i^{th} Leg of the Coupling

radius centered at A. This latter displacement is along the line which is the derivative of the spring with respect to θ_i, $\delta \underline{s}_i = -s_i \underline{i} + c_i \underline{j}$. Substituting these results into (2.17) provides the desired stiffness mapping

$$\begin{bmatrix} k_{11} & k_{12} \\ k_{21} & k_{22} \end{bmatrix} = \begin{bmatrix} c_1 & c_2 \\ s_1 & s_2 \end{bmatrix} \begin{bmatrix} k_1 & 0 \\ 0 & k_2 \end{bmatrix} \begin{bmatrix} c_1 & s_1 \\ c_2 & s_2 \end{bmatrix}$$

$$+ \begin{bmatrix} -s_1 & -s_2 \\ c_1 & c_2 \end{bmatrix} \begin{bmatrix} k_1(1-\rho_i) & 0 \\ 0 & k_2(1-\rho_2) \end{bmatrix} \begin{bmatrix} -s_1 & c_1 \\ -s_1 & c_2 \end{bmatrix} \tag{2.18}$$

This equation may be written compactly in the form

$$\delta \underline{f} = [K]\ \delta \underline{d}\ , \tag{2.19}$$

where from (2.18),

$$[K] = [j]\ [k_i]\ [j]^T + [\delta j]\ [k_i(1 - \rho_i)]\ [\delta j]^T, \tag{2.20}$$

where [j] is the formal instantaneous static Jacobian relating the differential change in the scalar spring forces to $\delta \underline{f}$, where $[\delta j]$ is its derivative with respect to θ_1 and θ_2, and where $[k_i]$ and $[k_i(1 - \rho_i)]$ are 2x2 diagonal matrices.[1]

[1]For observations about the matrix [K] and for its original derivation see Griffis[3].

CHAPTER 3
AN INVERSE FORCE ANALYSIS OF A PLANAR TWO-SPRING COUPLING

In this chapter, a closed-form inverse force analysis is performed on a planar two-spring coupling. The two springs are grounded to pivots at one end and attached to a common pivot at the other. A known force is applied to the common pivot of the system, and it is required to determine all of the assembly configurations. At the outset this appeared to be a relatively simple problem. However, this proved not to be the case. By variable elimination, a sixth degree polynomial in the resultant length of one spring is derived, and from this, six unique locations of the point of application of force are obtained. The results are verified numerically by performing a forward force analysis and displaying real solutions. It is clear that there are a maximum of six mathematical assembly configurations to obtain the desired force for such a spring system.[1]

This analysis is significant not only because it produces the exact number of assembly configurations, but also because it provides a simple tool for analyzing the quasi-static motion of the pivot as the desired applied force changes. In this chapter, the paths traced by the six roots are presented as the force changes along the F_X=F_Y spectrum. Using the stiffens mapping derived in Chapter 2, the stability of the system is also analyzed along these paths. Special cases with less than six real solution configurations are also discussed.

---

[1]Much of the material in this chapter has been previously presented by Pigoski and Duffy [15].

3.1 The Inverse Analysis Problem

The formulation of the inverse analysis problem is relatively simple. For the system shown in Figure 3.1, the spring elasticity constants (k_1 and k_2), the spring free lengths (l_{o1} and l_{o2}), and the distance between pivots A and B (d_{12}) are known a priori. It is required to compute all of the geometric configurations for specified forces F_x and F_y. This is accomplished by locating the pivot point P in terms of the resultant leg lengths of the configuration (l_1 and l_2) and the resultant leg rise angles (θ_1 and θ_2).

The resultant force at point P must be the sum of the forces created by the springs in the two legs. Mathematically, this can be represented by the following two equations:

$$F_x = k_1(l_1 - l_{o1})c_1 + k_2(l_2 - l_{o2})c_2 \tag{3.1}$$

$$F_y = k_1(l_1 - l_{o1})s_1 + k_2(l_2 - l_{o2})s_2 \tag{3.2}$$

where c_1, s_1, etc. represent the cosines and sines of their respective angles.

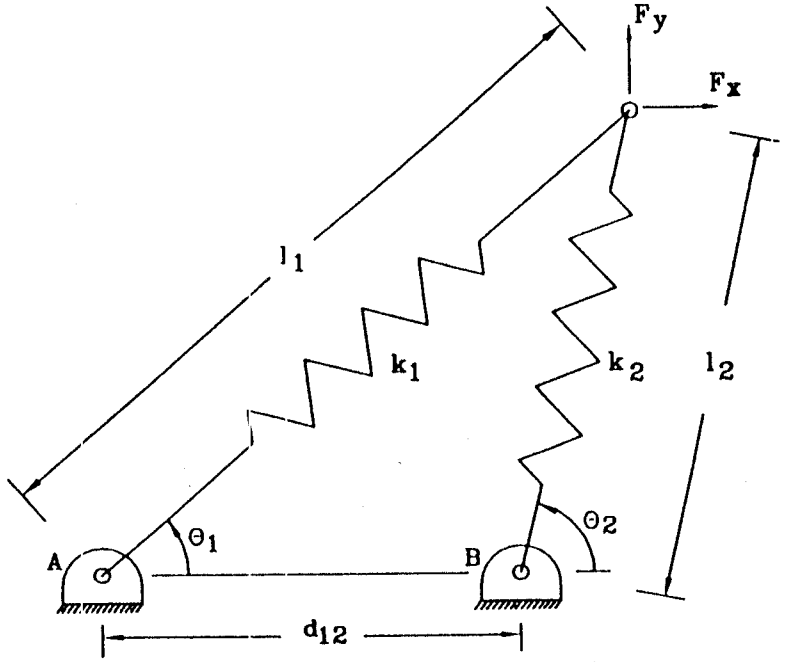

Figure 3.1 Planar Two-Spring Coupling

Additionally, the two equations which describe the geometry necessary for the legs to share a common pivot point are

$$l_2 s_2 = l_1 s_1 \tag{3.3}$$

$$l_2 c_2 = l_1 c_1 - d_{12} \tag{3.4}$$

These four independent equations completely describe the system and are sufficient to solve the problem. It should be noted that, in equations (3.1) and (3.2), the forces F_x and F_y are the reaction forces which must be applied at the pin to keep the system in equilibrium. The resultant forces (i.e. caused by the two springs) would be equal and opposite.

3.2 The Inverse Analysis Solution

It has been established that it is necessary to determine the location of the pivot point P in order to solve the inverse analysis problem. This can be accomplished by uniquely determining a leg length and subsequently the rise angle for either of the two legs. Here, two methods are presented to eliminate l_2 and θ_2 from equations (3.1) through (3.4) which result in a pair of independent equations containing l_1 and θ_1. Further elimination yields a sixth order polynomial in l_1.

The first elimination of l_2 and θ_2 is accomplished by rearranging (3.1) and (3.2) into the forms

$$F_x - k_1(l_1 - l_{o1})c_1 = k_2(l_2 - l_{o2})c_2 \tag{3.5}$$

$$F_y - k_1(l_1 - l_{o1})s_1 = k_2(l_2 - l_{o2})s_2 \tag{3.6}$$

which can be combined into the ratio

$$\frac{F_x - k_1(l_1 - l_{o1})c_1}{F_y - k_1(l_1 - l_{o1})s_1} = \frac{c_2}{s_2} . \tag{3.7}$$

Cross-multiplying and making the substitution $s_{2-1} = s_2c_1 - s_1c_2$ produces

$$F_x s_2 - F_y c_2 - k_1(l_1 - l_{o1})s_{2-1} = 0 . \tag{3.8}$$

From Figure 3.1, it is clear that

$$\frac{d_{12}}{s_{2-1}} = \frac{l_2}{s_1} . \tag{3.9}$$

Substituting (3.8) into (3.9) and rearranging gives

$$F_x l_2 s_2 - F_y l_2 c_2 - k_1(l_1 - l_{o1})d_{12}s_1 = 0 \tag{3.10}$$

Using (3.3) and (3.4) to eliminate l_2c_2 and l_2s_2 produces an equation which can be expressed in the form

$$A_1 s_1 + B_1 c_1 = D_1 \tag{3.11}$$

where

$$A_1 = F_x l_1 - k_1(l_1 - l_{o1})d_{12}$$

$$B_1 = -F_y l_1$$

$$D_1 = F_y d_{12}.$$

The second elimination begins by substituting for l_2c_2 and l_2s_2 in (3.1) and (3.2) using (3.3) and (3.4) which yields

$$F_x - Fc_1 + k_2 d_{12} = -k_2 l_{o2} c_2 \tag{3.12}$$

$$F_y - Fs_1 = -k_2 l_{o2} s_2 \tag{3.13}$$

where $F = \{(k_1+k_2)l_1 - k_1 l_{o1}\}$. Squaring and adding the left and right sides of (3.12) and (3.13) in order to eliminate θ_2 gives another equation which can be

expressed in the form

$$A_2 s_1 + B_2 c_1 = D_2 \tag{3.14}$$

where

$$A_2 = 2F_yF$$

$$B_2 = 2(F_x+k_2d_{12})F$$

$$D_2 = (F_x+k_2d_{12})^2+F_y^2+F^2 - k_2^2l_{o2}^2.$$

The coefficients in (3.11) and (3.14) are rearranged by firstly making the substitution $G = (F_x+k_2d_{12})$ and subsequently expressing A_1 in form

$$A_1 = F_xl_1 - k_1(l_1 - l_{o1})d_{12} - (k_2l_1d_{12}-k_2l_1d_{12})$$

$$= Gl_1 - Fd_{12}.$$

Equations (3.11) and (3.14) can thus be expressed in the form

$$A_i s_1 - B_i c_1 = D_i \qquad i = 1,2 \tag{3.15}$$

with the abbreviated coefficients

$$A_1 = Gl_1 - Fd_{12}$$

$$B_1 = - F_yl_1$$

$$D_1 = F_yd_{12}$$

$$A_2 = 2F_yF$$

$$B_2 = 2GF$$

$$D_2 = G^2+F_y^2+F^2-k_2^2l_{o2}^2$$

where $G = (F_x+k_2d_{12})$.

Eliminating θ_1 between the pair of equations (3.15) yields

$$(A_1B_2-A_2B_1)^2=(A_1D_2-A_2D_1)^2+(B_2D_1-B_1D_2)^2 \tag{3.16}$$

which is a function only of l_1 and known parameters.

Substitution of the coefficients of equations (3.15) into (3.16) results in the following sixth order polynomial:

$$a_6 l_1^6 + a_5 l_1^5 + a_4 l_1^4 + a_3 l_1^3 + a_2 l_1^2 + a_1 l_1 + a_0=0 \tag{3.18}$$

with coefficients

$$a_6 = - d_{12}^2(k_1+k_2)^6 + 2Gd_{12}(k_1+k_2)^5 - (G^2+F_y^2)(k_1+k_2)^4$$

$$a_5 = 6d_{12}^2k_1l_{o1}(k_1+k_2)^5-10Gd_{12}k_1l_{o1}(k_1+k_1)^4 + 4k_1l_{o1}(G^2+F_y^2)(k_1+k_2)^3$$

$$a_4 = d_{12}^2[2(2F_y^2+G^2-H)-15k_1^2l_{o1}^2] (k_1+k_1)^4$$

$$+ 4Gd_{12}[5k_1^2l_{o1}^2-2F_y^2-G^2+H] (k_1+k_2)^3+ 2[G^2(3F_y^2+G^2$$

$$-H)+F_y^2(F_y^2+k_2^2l_{o2}^2) - 3(G^2+F_y^2)k_1^2l_{o1}^2](k_1+k_2)^2$$

$$a_3 = 4d_{12}^2k_1l_{o1}[5k_1^2l_{o1}^2-4F_y^2-2G^2+2H](k_1+k_2)^3 - 4Gd_{12}k_1l_{o1}[5k_1^2l_{o1}^2$$

$$-6F_y^2-3G^2+3H](k_1+k_2)^2+4k_1l_{o1}[k_1^2l_{o1}^2(G^2+F_y^2)-G^2(3F_y^2+G^2-H)$$

$$- F_y^2(F_y^2+k_2^2l_{o2}^2)](k_1+k_2)$$

$$a_2 = \{3d_{12}^2k_1^2l_{o1}^2[4(2F_y^2+G^2-H)-5k_1^2l_{o1}^2] - d_{12}^2(G^4+H^2+2G^2H$$

$$+4F_y^2k_2^2l_{o2}^2)\}(k_1+k_2)^2 + \{2Gd_{12}k_1^2l_{o1}^2[5k_1^2l_{o1}^2$$

$$-6(2F^2+G^2-H)] + 2Gd_{12}[G^4+H^2+2G^2H]\}(k_1+k_2)$$

$$-(G^2+F_y^2)k_1^4 l_{o1}^4 + [2G^2(3F_y^2+G^2-H)+2F_y^2(F_y^2+k_2^2 l_{o2}^2)]k_1^2 l_{o1}^2$$

$$-(G^2+F_y^2)(G^4+H^2+2G^2H)$$

$$a_1 = 2d_{12}^2 k_1 l_{o1}\{k^2 l_{o1}^2[3k_1^2 l_{o1}^2-4(2F_y^2+G^2-H)] +[G^4+H^2+2G^2H$$

$$+4F_y^2 k_2^2 l_{o2}^2]\}(k_1+k_2) - 2Gd_{12}k_1^5 l_{o1}^5$$

$$+4Gd_{12}(2F_y^2+G^2-H)k_1^3 l_{o1}^3 - 2Gd_{12}k_1 l_{o1}[G^4+H^2+2G^2H]$$

$$a_0 = -d_{12}^2 k_1^6 l_{o1}^6+2d_{12}^2(2F_y^2+G^2-H)k_1^4 l_{o1}^4$$

$$-d_{12}^2 k_1^2 l_{o1}^2(G^4+H^2+2G^2H+4F_y^2 k_2^2 l_{o2}^2)$$

where $G = F_x+k_2 d_{12}$ and $H = F_y^2-k_2^2 l_{o2}^2$.

3.3 A Numerical Inverse Force Example

Here a numerical example is given which yields six real solutions. A coordinate system fixed at point A and oriented in such a manner that the distance d_{12} lies along the x-axis was chosen, and the system constants were as follows: $k_1 = 1.000$, $k_2 = 1.500$, $l_{o1} = 1.000$, $l_{o2} = 1.500$, and $d_{12} = 1.000$. Solutions were obtained to produce the forces, $F_x = F_y = 0.25$ units, acting on the pivot P.

Substituting the above values into equation (3.18), the following monic polynomial was obtained:

$$l_1^6 - 4.000...l_1^5 + 3.780...l_1^4 + 3.264...l_1^3 - 7.045...l_1^2 + 3.398...l_1 - 0.424... = 0,$$

which has the following six real roots:

$$l_1 = 0.196..., 0.624..., 1.109..., 1.791..., 1.470..., -1.190...$$

Corresponding real values of θ_1 were obtained from the pair of equations (3.15). Substitution into equations (3.12) and (3.13) then produced corresponding real values for θ_2. Finally, the corresponding six real values for l_2 were obtained from equations (3.3) and (3.4). The six solution sets to this problem are as follows:

1: l_1=0.196..., l_2=0.811..., θ_1=346.3..., θ_2=183.3...

2: l_1=0.624..., l_2=1.517..., θ_1=223.2..., θ_2=196.3...

3: l_1=1.109..., l_2=1.225..., θ_1=289.2..., θ_2=238.8...

4: l_1=1.791..., l_2=0.997..., θ_1=343.8..., θ_2=308.5...

5: l_1=1.470..., l_2=1.379..., θ_1=295.3..., θ_2=105.6...

6: l_1=-1.190..., l_2=0.192..., θ_1=178.6..., θ_2=351.1...

These yielded the following corresponding locations of the pivot point P with respect to the coordinate system described above:

1: (x_p = 0.190..., y_p = -0.046...)

2: (x_p = -0.455.., y_p = -0.427...)

3: (x_p = 0.365..., y_p = -1.047...)

4: (x_p = 1.607..., y_p = -0.791...)

5: (x_p = 0.629..., y_p = 1.328...)

6: (x_p = 1.189..., y_p = -0.030...) .

All six of these solutions are real achievable geometric configurations, and a simple forward analysis was performed to verify their accuracy. Figure 3.2 shows these solutions labeled with the applied force for static equilibrium. In Figure 3.2-6, a broken line is used to denote l_1 is a negative spring length.

3.4 The Significance of Negative Spring Lengths

In the above example, the sixth solution yields a negative spring length, l_1=-1.190. Given the polar nature of the coordinates (l_1,θ_1) used to determine the rectilinear coordinates of point P, the meaning of the negative value of l_1 obtained from the sixth-degree polynomial was not immediately clear. However, a negative spring length can be realized physically by considering a spring compressed through its own fixed pivot. In the above example, when P is forced to pass through A, the spring k_1 has a negative spring length. It should thus be clear that a spring with a negative length is in compression.

It is important to note that in Figure 3.2-6, the polar coordinates for the pivot P are (-1.190 units, 178.6 deg), and the equilibrant force components are F_x = F_y = 0.25 units. In this solution, leg 1 is providing a force equal to -2.190 units (= $k_1(l_1-l_{o1})$) at an angle of 178.6 degrees, θ_1. Precisely the same triangular solution configuration can be obtained using the polar coordinates (1.190 units, 358.6 deg). However, the resultant force in leg 1 would be 0.190 units at 358.6 degrees rather than the desired force. In the case of the latter, the equilibrant applied force components necessary are not F_x = F_y = 0.25 units but F_x = -1.748 and F_y = 0.289 units.

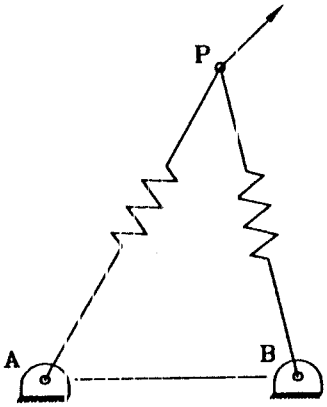

Figure 3.2-1

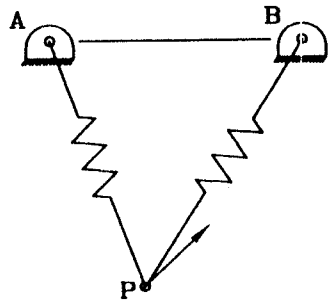

Figure 3.2-2

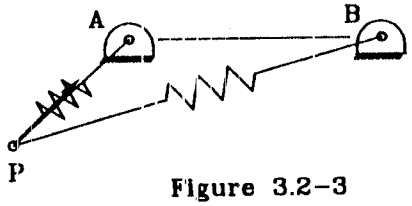

Figure 3.2-3

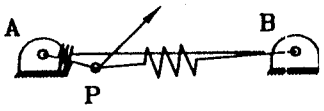

Figure 3.2-4

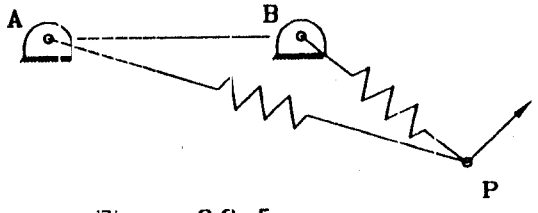

Figure 3.2-5

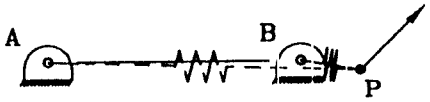

Figure 3.2-6

Figure 3.2 System Configurations at $F_x = F_y = 0.25$

Although not commonly used for problems of this sort, springs which can achieve negative lengths can be conceived. A spiral spring under axial load will pass through a zero length position without changing force direction. As mentioned above, springs with a negative length are under a compressive load and will inherently become increasingly unstable as the load increases. It should be noted, however, that no engineering solutions for the design of stable springs in compression which will avoid possible buckling are presented here.

Additionally, the inclusion of negative spring lengths into spring problems has a significant impact on their forward analysis. Referring back to Figure 3.1, given the location of point P via x_p and y_p, spring lengths l_1 and l_2 can be obtained by solving the equations:

$$l_1 = \pm(x_p^2 + y_p^2)^{1/2} \quad \text{and} \quad l_2 = \pm((x_p - d_{12})^2 + y_p^2)^{1/2}.$$

Traditional forward analysis considers only the positive solutions and thus produces a single resultant force for each location in the plane of point P. When negative spring lengths are introduced into the analysis, it is clear that there exist four possible resultant forces for each location of point P corresponding to the four combinations of the positive and negative lengths of l_1 and l_2. The angles necessary to complete the solution sets are obtained from the polar equations:

$$x_p = l_1 \cos\theta_1, \quad y_p = l_1 \sin\theta_1, \quad x_p - d = l_2 \cos\theta_2, \quad \text{and} \quad y_p = l_2 \sin\theta_2.$$

This result implies that, for any n-spring system in the plane (or in space), a forward analysis will have 2^n (i.e. 2 for each leg) solutions including single solution obtained from a traditional forward analysis.

3.5 Quasi-Static Path Tracing

For the above example six solutions were also found for a zero applied force. These unloaded configurations are illustrated in Figure 3.3. Two solutions occur when the moving pivot is coincident with the points labeled R and S in Figure 3.3. These configurations are the resultant geometries formed by the free lengths of the two springs and are obviously symmetric about the line joining the fixed pivots A and B. Additionally, four solutions occur on the line joining A and B when the moving pivot P is located at points T, U, V, and W.

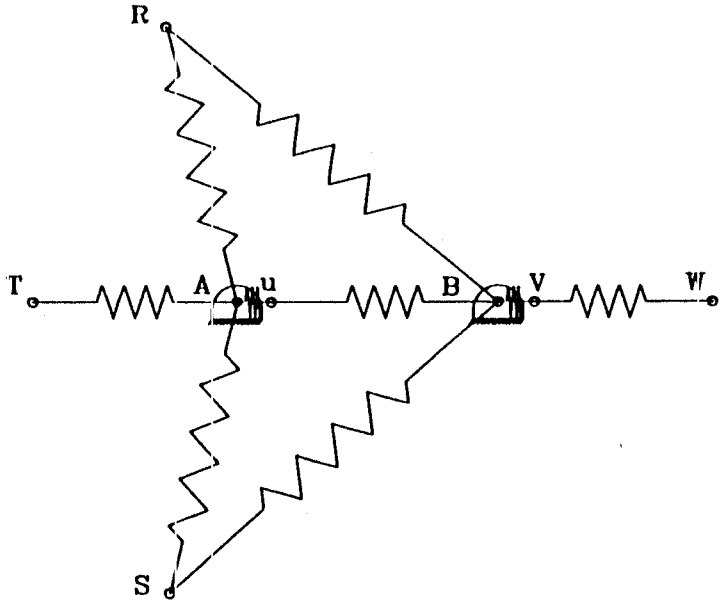

Figure 3.3 Configurations for a Zero-Load Resultant

The six possible paths traced by the moving pivot are illustrated in Figure 3.4. These were obtained by incrementing the applied force starting at the zero applied force configurations. The direction of the applied force was held constant at 45 degrees. The six distinct paths traced by the pivot P are labeled CF1 through CF6. The six distinct configurations for $F_x = F_y = 0.25$ unit which

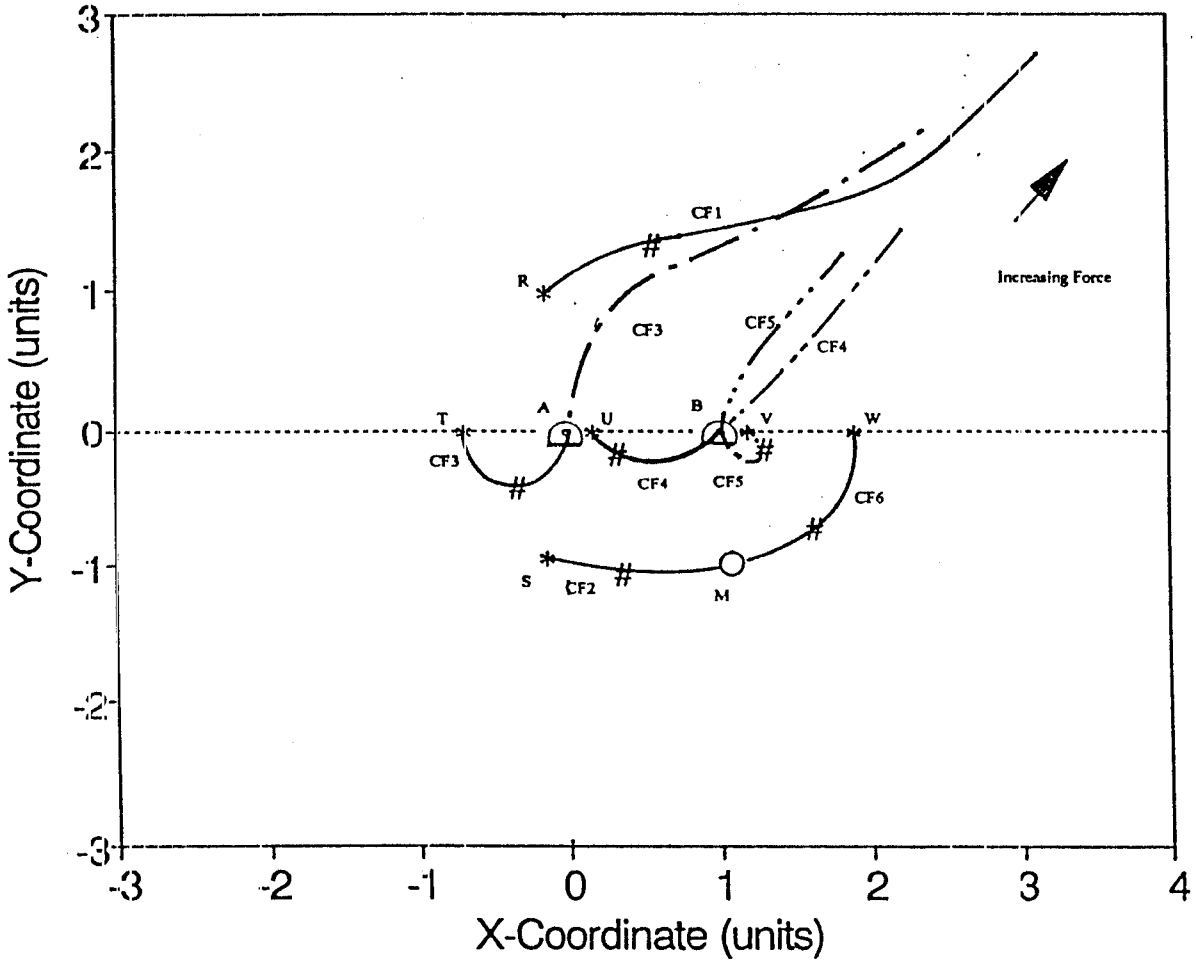

Figure 3.4 Pivot Motion Caused by an Increasing Applied Force

are labeled on each path by a number sign (#) in Figure 3.4 are in complete agreement with the configurations in Figure 3.2. Further the six distinct configurations for $F_x = F_y = 0$ are marked with an asterisk and are labeled R through W as they are in Figure 3.3.

The broken lines indicate that either one or both leg lengths are negative. A single dot indicates leg 1 has a negative length, two dots indicate leg 2 has a negative length, and three dots indicate both legs do. It should be clear from Figure 3.4 that as the curve CF3 passes through the fixed pivot A, leg length l_1 (which is pivoted at A) must become negative, and similarly, as the curve CF4 passes through the fixed pivot B, leg length l_2 must become negative. On the curve CF5, leg length l_1 is always negative, and leg length l_2 becomes negative as point P passes through pivot B.

An interesting phenomena appears in Figure 3.4. Curves CF3, CF4, and CF6 indicate that the pivot point P moves in a direction opposite to that which one would expect as the force is incremented from zero. Intuitively, this would indicate an instability in the system. Stability can be determined from the signature of the system's 2X2 symmetric stiffness matrix [K] at each point on each curve. Briefly, the stiffness mapping is used to correlate a small change in applied force into a corresponding motion by the relation:

$$\begin{bmatrix} \delta F_x \\ \delta F_y \end{bmatrix} = [K] \begin{bmatrix} \delta x \\ \delta y \end{bmatrix}$$

where as derived in chapter 2:

$$[K] = \begin{bmatrix} k_{11} & k_{12} \\ k_{12} & k_{22} \end{bmatrix} = \begin{bmatrix} c_1 & c_2 \\ s_1 & s_2 \end{bmatrix} \begin{bmatrix} k_1 & 0 \\ 0 & k_2 \end{bmatrix} \begin{bmatrix} c_1 & s_1 \\ c_2 & s_2 \end{bmatrix}$$

$$+ \begin{bmatrix} -s_1 & -s_2 \\ c_1 & c_2 \end{bmatrix} \begin{bmatrix} k_1(1-\rho_1) & 0 \\ 0 & k_2(1-\rho_2) \end{bmatrix} \begin{bmatrix} -s_1 & c_1 \\ -s_2 & c_2 \end{bmatrix}$$

and $\rho_i = l_i/l_{oi}$. The signature of [K] indicates the possibilities of change of state of potential energy in the system. The signature can be represented as (π, ν, ζ) and is defined as the number of positive, negative, and zero eigenvalues of the stiffness matrix. For example, at a point on a curve when [K] is positive definite(2,0,0), the potential energy is concave up for all incremental displacements (a local minimum), and the configuration is stable. A signature of (1,1,0) indicates a configuration of limited stability (a saddle point). A signature of (0,2,0) indicates an unstable configuration for which the potential energy is concave-down (a local maximum) (see Griffis[4]).

Figure 3.5 illustrates the stability of the system along the coordinate paths traced by Figure 3.4. Broken lines indicate configurations of limited stability and solid lines indicate stable configurations. It is interesting to note that stable configurations exist along curves CF3, CF4, and CF5 which contain negative spring lengths. Additionally, at the system's unloaded configurations which are labeled R through W, as expected, the system is stable at Points R and S corresponding to the geometry of the system at the free lengths of the springs, and it has limited stability when the pivot is at points T through W. This limited stability derives from the fact that the system would be stable against a force applied purely in the x direction but unstable against any other force.

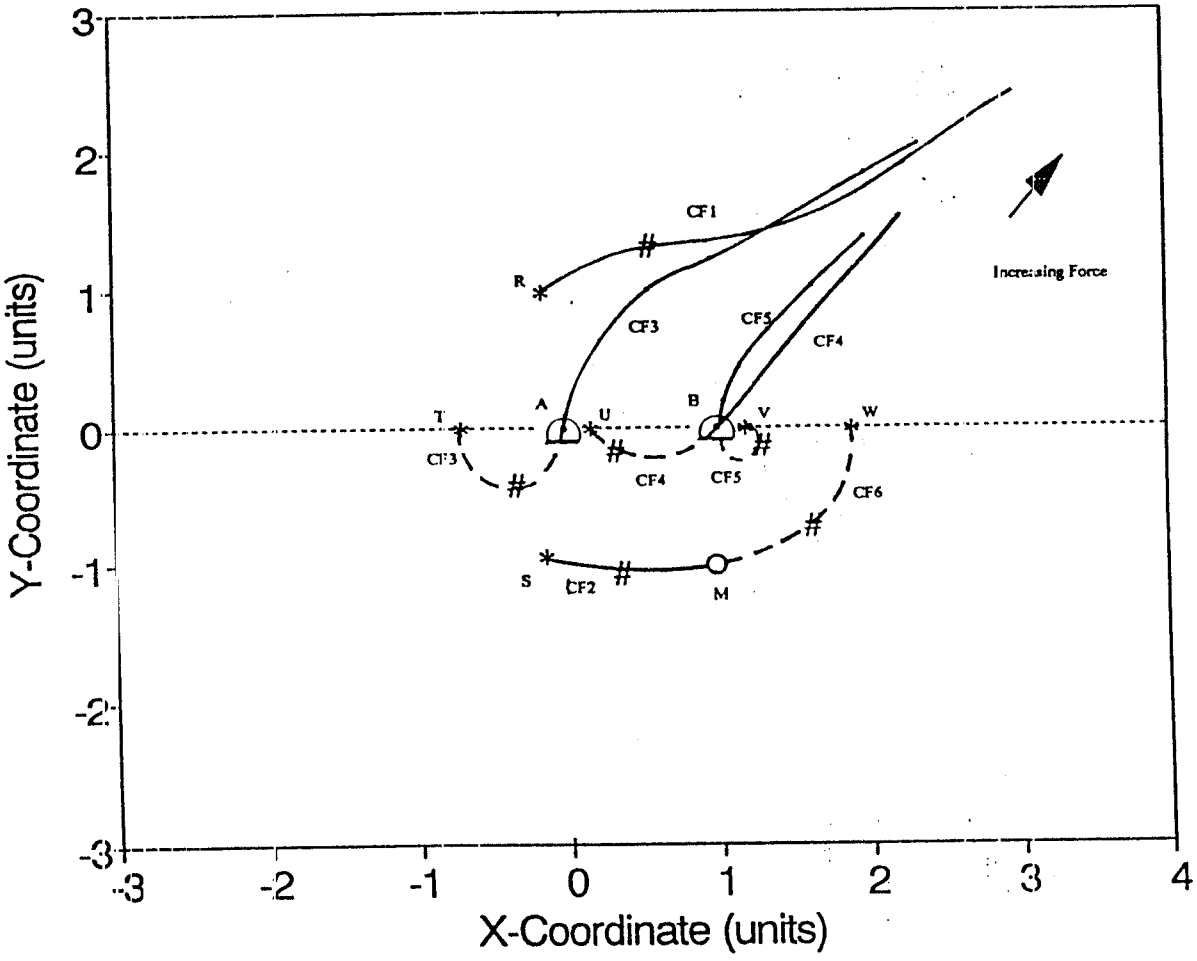

Figure 3.5 System Stability Along Configuration Paths

It is of further interest to discuss the apparent merger of the traces CF2 and CF6 at the point M, the coordinates for which are approximately (0.811, -1.080) and $F_x = F_y = 0.317$. Referring to Figure 3.4, consider the pivot P is at the unloaded stable position S. As the force is increased incrementally from zero, the pivot moves along the curve CF2 until it is at point M. If the force is increased above $F_x = F_y = 0.317$, two of the roots of the sixth order polynomial in l_1 become complex, and only four real solutions exist. From Figure 3.5 it is clear that M is a point of change of stability of the system. However, more insight can be obtained by examining the potential energy of the system with respect to the applied force. Figure 3.6 shows the potential energy of the system with respect to the applied force along curves CF2 and CF6. At point M the slope of both curves goes to infinity indicating no change in potential energy would counter the increase in force. It can be deduced that, in this configuration, the system is highly unstable and will behave unpredictably.

For the sake of geometric symmetry, an incremental force acting in the opposite direction was also applied to the pivot point P. Figure 3.7 shows the six paths traced by the pivot under this load, again the assembly configurations are labeled consistently with Figure 3.4. The system exhibits the same type of behavior with leg lengths clearly becoming negative, and it shows another instability point (also labeled M) where curves CF1 and CF3 come together. Figure 3.8 combines Figures 3.4 and 3.7 and yields the complete picture. Finally, Figure 3.9 shows stability along these paths.

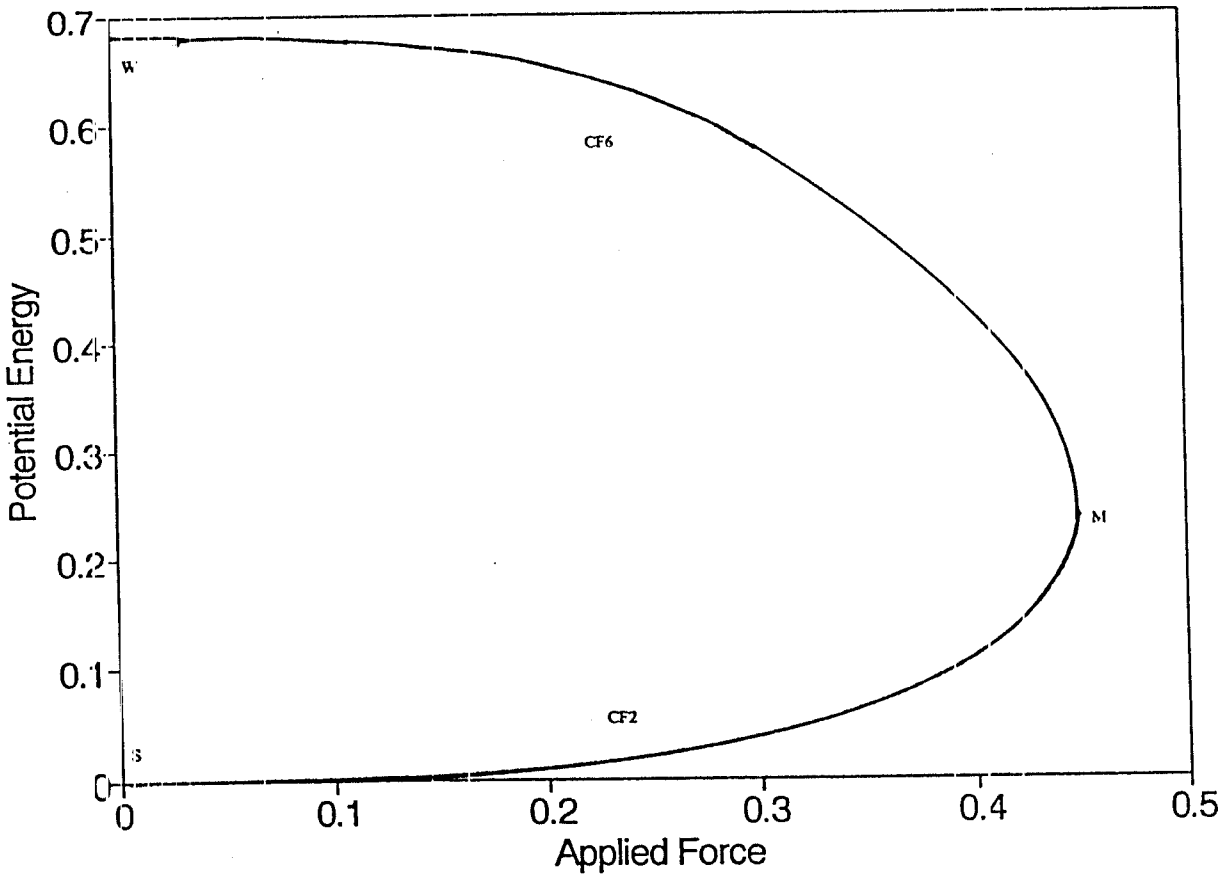

Figure 3.6 Potential Energy as the Pivot Approaches a Complex Point

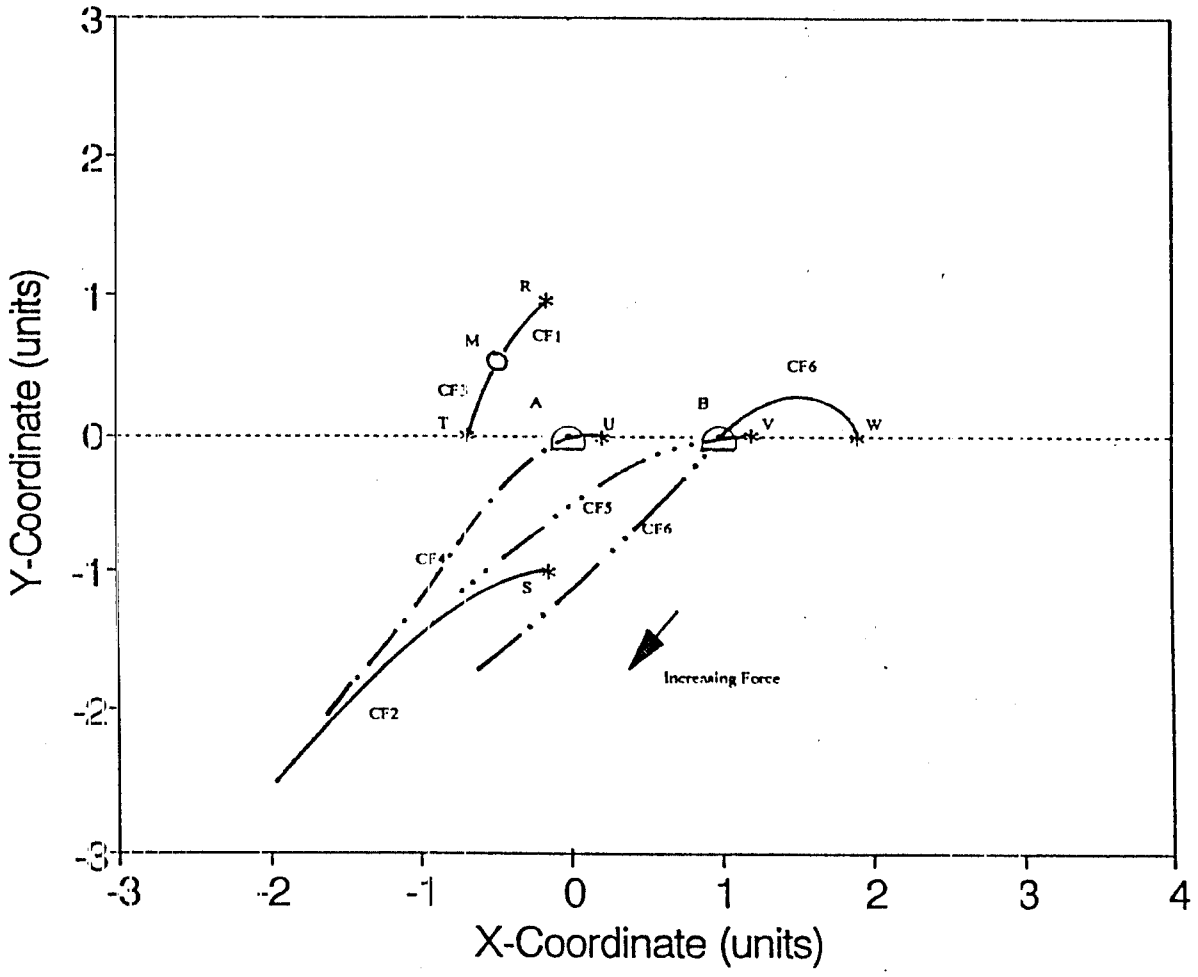

Figure 3.7 Pivot Motion Caused by an Increasing Force in the Negative Direction

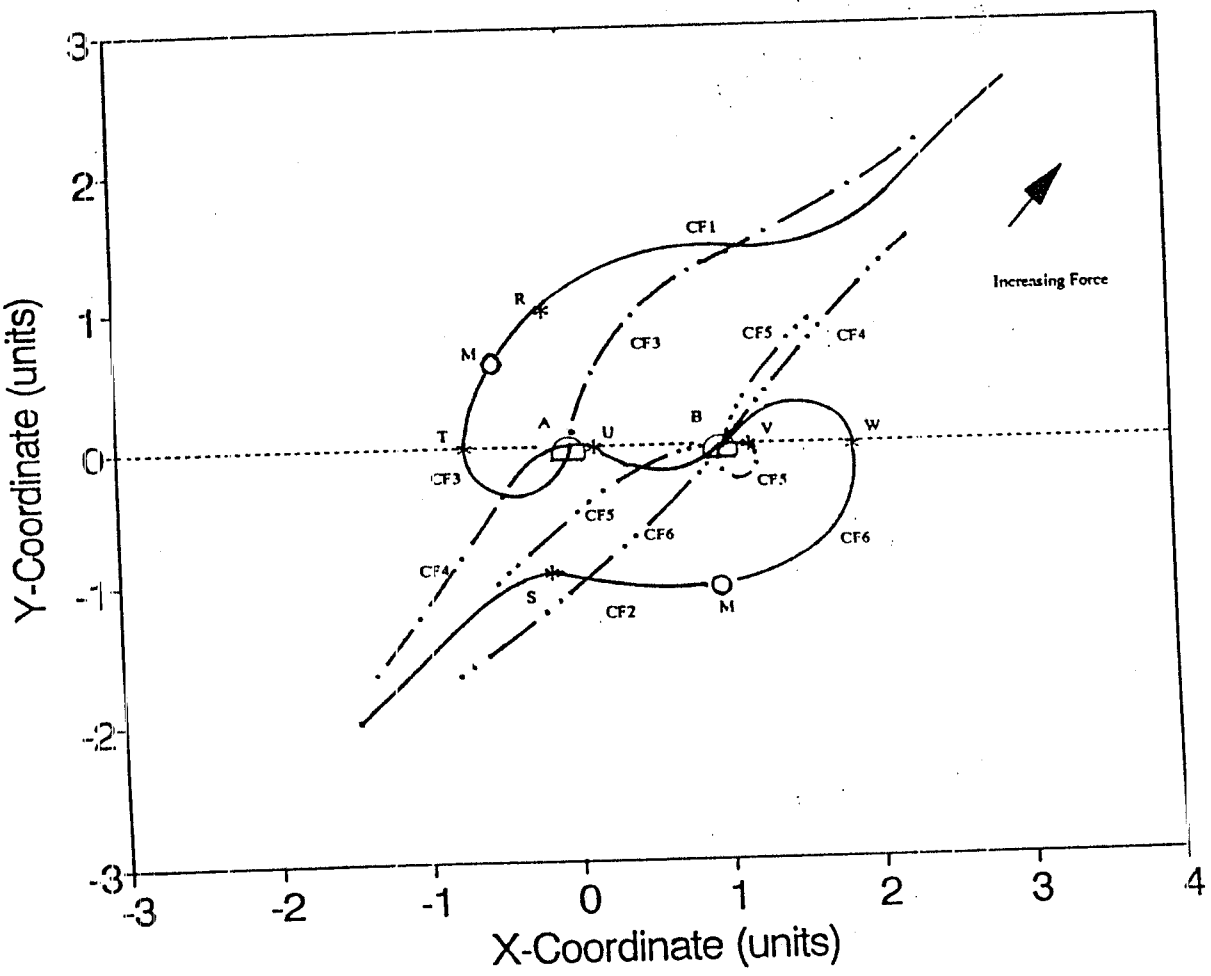

Figure 3.8 Pivot Motion for the $F_x = F_y$ Spectrum

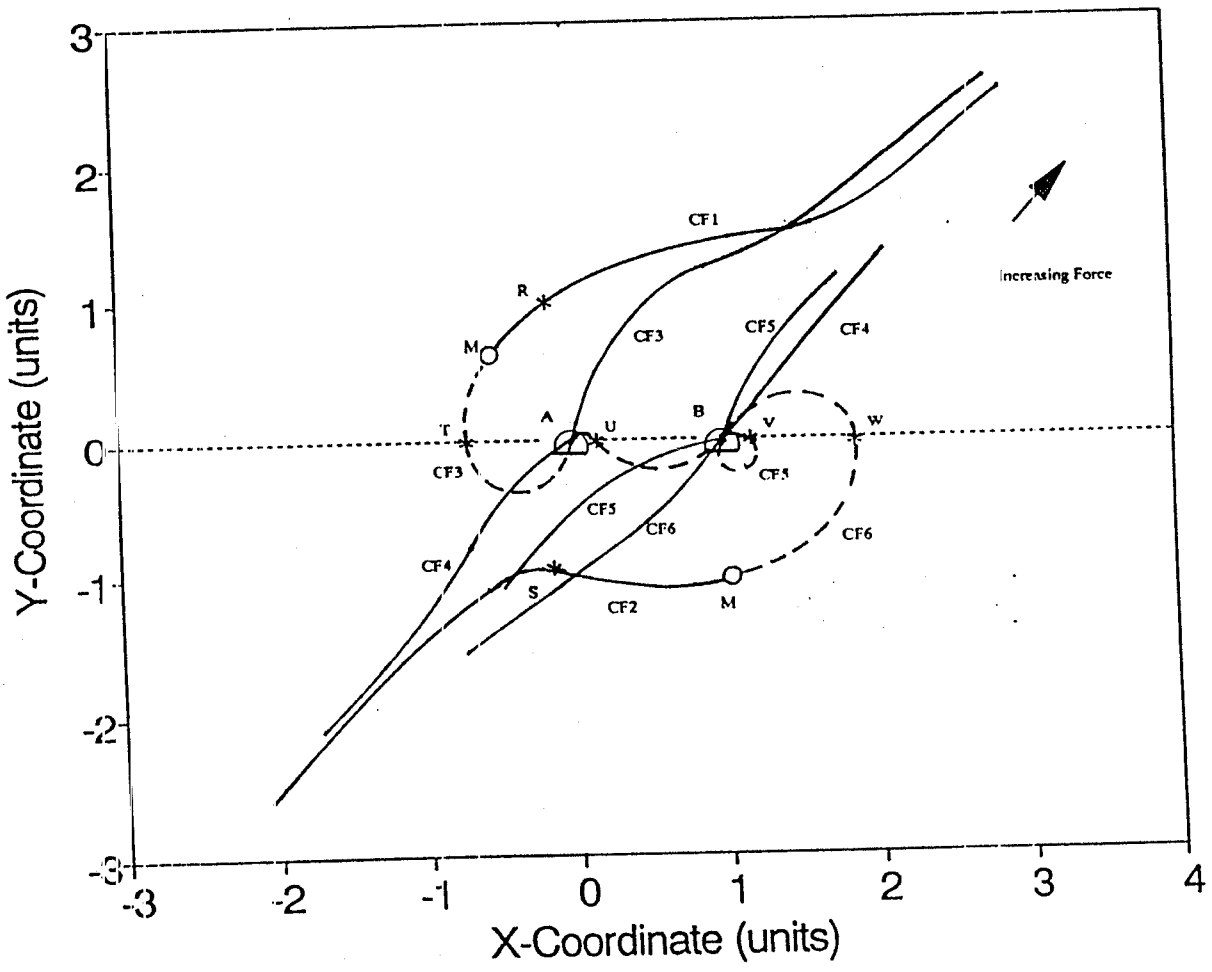

Figure 3.9 System Stability Along the $F_x = F_y$ Configurations

3.6 Special Cases not Yielding Six Real Solutions

The above example exhibited the most general behavior possible for a planar two-parameter spring. Six real configurations were obtained under a zero force condition. Four configurations occurred along the line joining the two pivots, and two occurred at free lengths of the springs. If, however, the condition that $l_{o1}+l_{o2}<d_{12}$ exists, this latter pair cannot exist in the real plane, and a set of complex conjugates in l_1 is obtained from the sixth-order polynomial at zero force. It is speculated that for such systems only a maximum of four real solutions can ever exist regardless of the magnitude of the applied force. Figure 3.10 shows the motion of the pivot for an example where $l_{o1}+l_{o2}=d_{12}$. At the zero-force solution indicated by S, l_1 equals l_{o1}, and this is a triple root in the solution of the sixth order polynomial. Two of these three solutions become complex for any other applied force. The third set of solutions is the curve which passes through S in Figure 3.10. These systems are stable for all configurations shown.

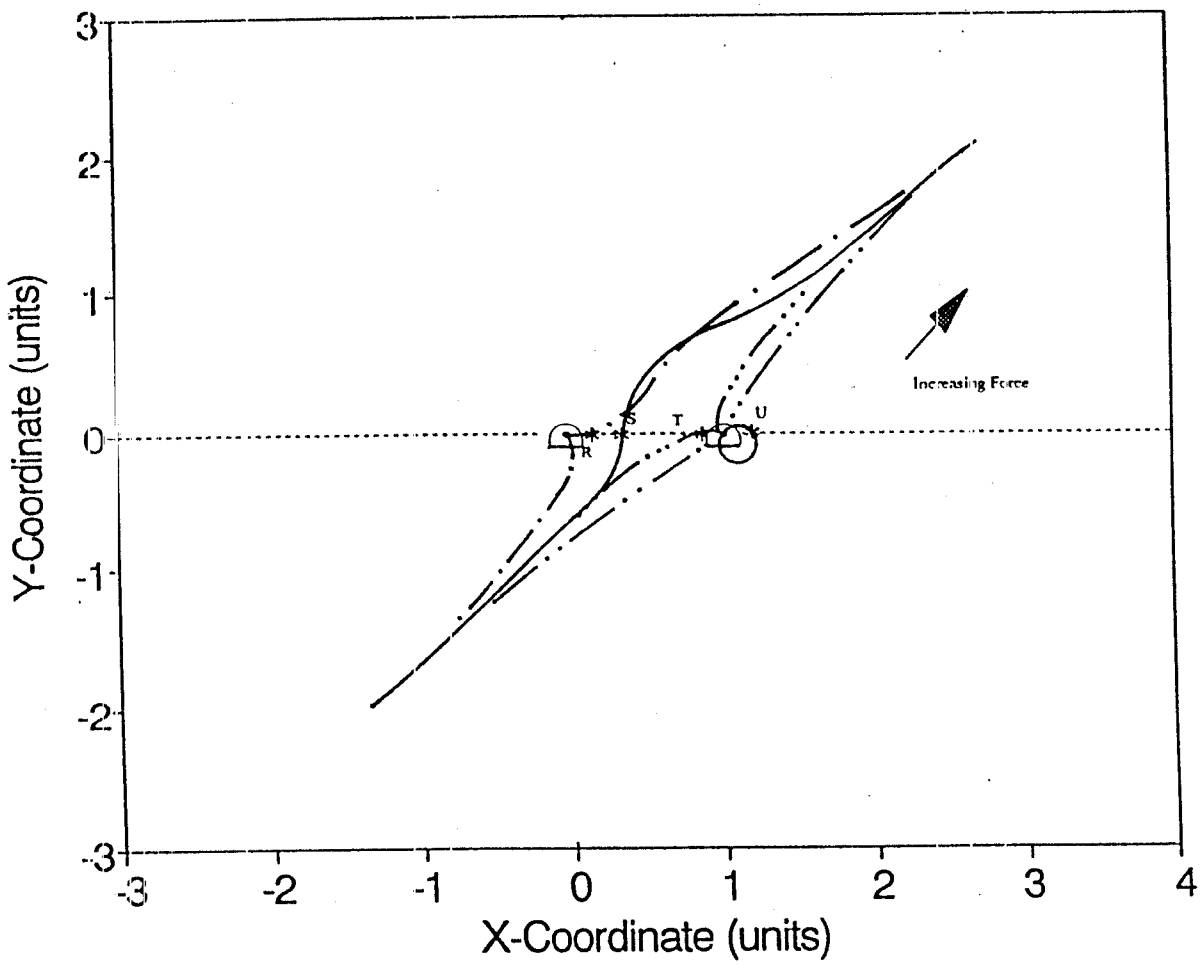

Figure 3.10 Pivot Motion Caused by an Increasing Applied Force when $l_{o1} + l_{o2} = d_{12}$

CHAPTER 4
FRAME OF REFERENCE-DEPENDENT STIFFNESS MAPPINGS FOR A PLANAR THREE-SPRING COUPLING

The spatial stiffness of a compliant coupling which connects two bodies is used to map a small relative twist into a corresponding interactive wrench increment (see Griffis and Duffy[5], Griffis[3]). In its general form, the mapping is

$$\delta\hat{w} = [K]\ \delta\hat{D}\ , \tag{4.1}$$

where $\delta\hat{w}$ are the coordinates of a wrench increment, $\delta\hat{D}$ are the coordinates of an infinitesimal twist, and [K] is the stiffness matrix, which in general is a 6x6 asymmetric matrix whose elements are dependent upon the geometrical and material stiffness properties of the coupling.

In this chapter, the stiffness mapping matrix for the planar three-spring coupling shown in Figure 4.1 is analyzed using two different reference frames. The first is rigidly attached to the fixed body of the coupling (see Griffis and Duffy[16]), while the second is attached to the moving body of the coupling. It is found that these matrices are asymmetric when the coupling is loaded, and that one is the transpose of the other. This important result can be considered an extension of the work done by Dimentberg[6], who derived a symmetrical stiffness mapping for an unloaded coupling. These new mappings are essential for the control of the coupling as it moves away from its unloaded position.[1]

---

[1]Much of the material presented in this chapter has been previously presented by Pigoski, Griffis, and Duffy[17].

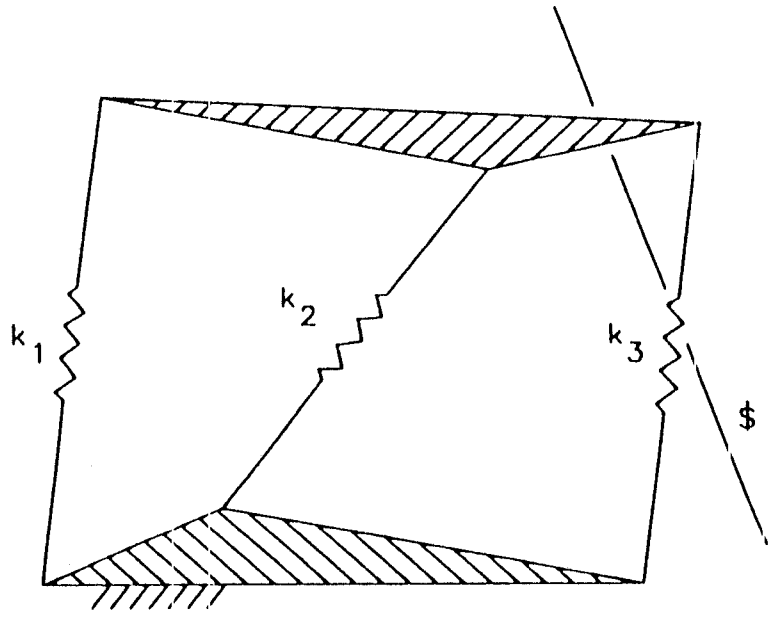

Figure 4.1 Planar Three-Spring Coupling

Additionally, a third frame of reference which undergoes rectilinear motion with respect to the fixed body and is hinged to the moving body is analyzed. This frame always produces a symmetric mapping and is found to be identical to the Hessian matrix obtained from the second differentials of the elastic potential energy of the system. (see Loncaric[[12]) The impetus for including this reference frame was the appearance of the asymmetries in the above reference frames which at the outset appeared to be incompatible with previously reported symmetric mappings. Additionally, Loncaric[18] has shown that for any generalized spring system, a coordinate system can be chosen which will lead to a simplified form of its stiffness matrix. However, this simple symmetric mapping cannot be used directly in a control algorithm such a that detailed in [3] and [5] since no force\torque sensor can be mounted in this reference frame. It is only included to show that such a frame can be realized.

exists. Finally, static force loci for each of the reference frames are drawn to support the notion of frame-of-reference dependency.

4.1 Fixed-Body Stiffness Mapping

Referring to the coupling shown in Figure 4.2, it is required to determine a mapping that relates the axis through point P of a $\delta\phi$ rotation to a line $\$_a$ of a force (δf) increment in the static force applied to the moving body. (It is considered that $\delta\phi$ is small so that $\delta\phi \rightarrow 0$.) In this section, this mapping is referenced to the fixed body, which means that the two external static forces which keep the moving body in static equilibrium before and after the $\delta\phi$ rotation are referenced to (or are drawn in) the fixed body. The difference in these two static forces is the force increment that occurs along the line $\$_a$.

Here, expressed in terms of an xy coordinate system that is located at some point O in the fixed body, this mapping is

$$\delta\hat{w}_O = [K_O]\ \delta\hat{D}_O, \tag{4.2}$$

where the coordinates of the force increment are $\delta\hat{w}_O = [\delta F_x,\ \delta F_y;\ \delta m_O]^T$, the coordinates of the $\delta\phi$ rotation are $\delta\hat{D}_O = [\delta x_O,\ \delta y_O;\ \delta\phi]^T$, and $[K_O]$ is a 3x3 stiffness matrix. Before the $\delta\phi$ rotation, the static force applied to the moving body required to keep it in static equilibrium is given by the coordinates, $\hat{w}_O = [F_x,\ F_y;\ m_O]^T$, whereas after the $\delta\phi$ rotation, the new static force is given by the coordinates $\hat{w}_O^+ = [F_x^+,\ F_y^+;\ m_O^+]^T$. (The three coordinates of a force denote the projections of the force onto the x and y axes and the moment of the force about the point O.) The coordinates of the force increment referenced to the fixed body are then obtained from

$$\delta\hat{w}_O = \hat{w}_O^+ - \hat{w}_O\ , \tag{4.3}$$

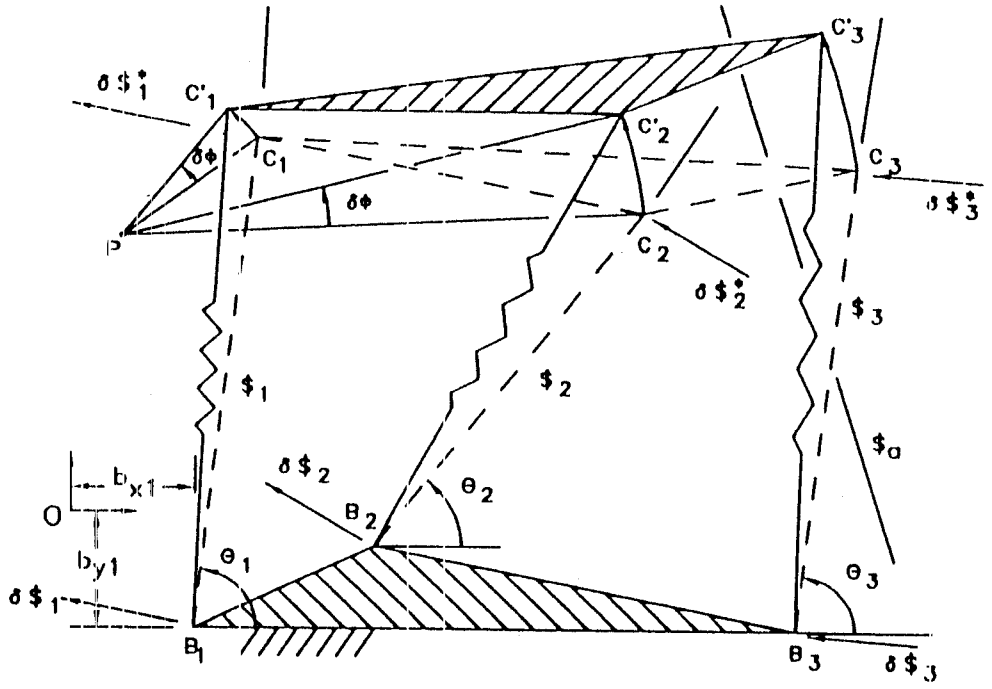

Figure 4.2 Motion of the Platform with respect to a Reference Frame in the Fixed Body

where $\delta F_x = F_x^+ - F_x$, $\delta F_y = F_y^+ - F_y$, and $\delta m_o = m_o^+ - m_o$.

The infinitesimal displacements δx_o and δy_o are of the point in the moving body that is coincident with O, while the infinitesimal rotation $\delta\phi$ denotes a change in orientation of the moving body relative to the fixed body. These three coordinates taken together form $\delta\hat{D}_o$, which locates an axis of rotation through the point P, whose coordinates x_p and y_p are obtained from

$$x_p = -\delta y_o/\delta\phi \text{ and } y_p = \delta x_o/\delta\phi. \tag{4.4}$$

When the axis of rotation is quantified by the coordinates $\hat{S}_o = [y_p, -x_p; 1]^T$, then the $\delta\phi$ rotation can be expressed as the scalar multiple

$$\delta \hat{D}_o = \delta\phi \, \hat{S}_o. \tag{4.5}$$

In order to derive the mapping of stiffness (4.2), it is necessary to first express the external static force applied to the moving platform as the resultant of the forces in the springs, f_1, f_2, and f_3:

$$\hat{w}_o = f_1 \hat{s}_1 + f_2 \hat{s}_2 + f_3 \hat{s}_3, \tag{4.6}$$

where $\hat{s}_i = [c_i, s_i; r_i]^T$ are the coordinates (direction cosines and perpendicular distance from O) of the line $\$_i$ of the i^{th} spring. (Refer to Figure 4.3, $c_i = \cos(\theta_i)$, $s_i = \sin(\theta_i)$, and $r_i = b_{xi}\, s_i - b_{yi}\, c_i$, where b_{xi} and b_{yi} are the coordinates of the fixed pivot point B_i.) Substituting into (4.6) the relations $f_i = k_i(l_i - l_{oi})$, where k_i and $(l_i - l_{oi})$ are respectively the spring constant and difference between the current and free lengths of the i^{th} spring, yields

$$\hat{w}_o = k_1(l_1 - l_{o1})\, \hat{s}_1 + k_2(l_2 - l_{o2})\, \hat{s}_2 + k_3(l_3 - l_{o3})\, \hat{s}_3. \tag{4.7}$$

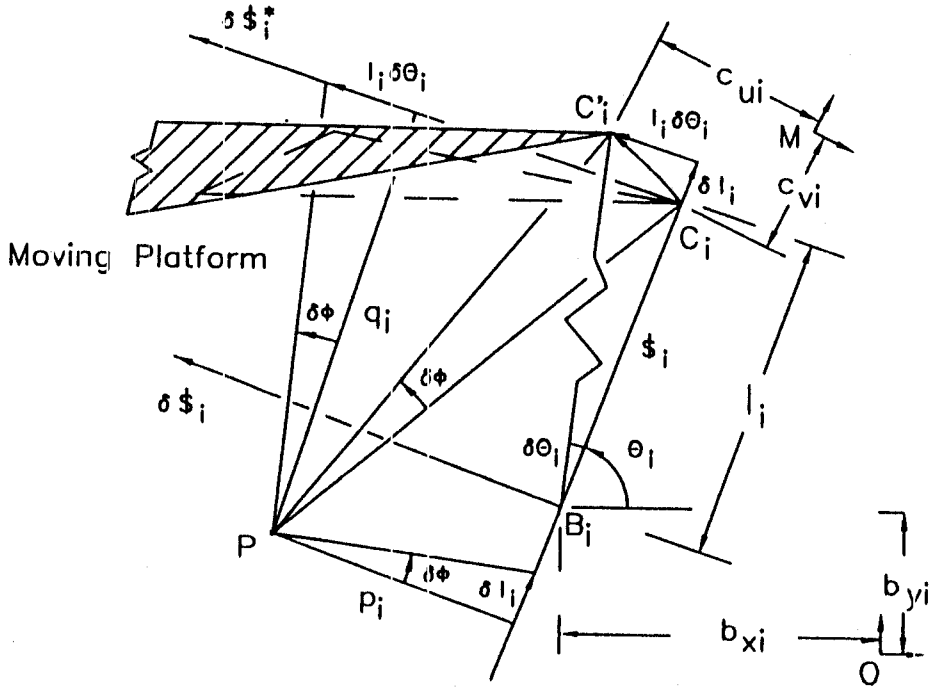

Figure 4.3 Motion of an i^{th} Leg of the Coupling

Successive applications of (4.7), which yields $\hat{w}_o$ and $\hat{w}_o^+$, could provide the coordinates of force increment. However, in order to obtain the mapping (4.2), it is desirable to differentiate (4.7), which yields

$$\delta\hat{w}_o = k_1\,\delta l_1\,\hat{s}_1 + k_2\,\delta l_2\,\hat{s}_2 + k_3\,\delta l_3\,\hat{s}_3 +$$

$$k_1(l_1 - l_{o1})\,\frac{\delta\hat{s}_1}{\delta\theta_1}\,\delta\theta_1 + k_2(l_2 - l_{o2})\,\frac{\delta\hat{s}_2}{\delta\theta_2}\,\delta\theta_2 + k_3(l_3 - l_{o3})\,\frac{\delta\hat{s}_3}{\delta\theta_3}\,\delta\theta_3. \qquad (4.8)$$

The coordinates, $\frac{\delta\hat{s}_i}{\delta\theta_i} = [-s_i,\ c_i,\ \delta r_i]^T$ (where $\delta r_i = b_{xi}\,c_i + b_{yi}\,s_i$), locate a line $\delta\$_i$ that is perpendicular to the line of the spring $\$_i$ at that line's fixed pivot point B_i, and therefore, the line $\delta\$_i$ is defined as the geometric derivative of $\$_i$ referenced to the fixed body. (See Figures 4.2 and 4.3.) An equivalent form of (4.8) is

$$\delta\hat{w}_o = k_1\,\delta l_1\,\hat{s}_1 + k_2\,\delta l_2\,\hat{s}_2 + k_3\,\delta l_3\,\hat{s}_3 +$$

$$k_1(1 - \rho_1)\,\frac{\delta\hat{s}_1}{\delta\theta_1}\,l_1\,\delta\theta_1 + k_2(1 - \rho_2)\,\frac{\delta\hat{s}_2}{\delta\theta_2}\,l_2\,\delta\theta_2 + k_3(1 - \rho_3)\,\frac{\delta\hat{s}_3}{\delta\theta_3}\,l_3\,\delta\theta_3, \quad (4.9)$$

where the parameters, $\rho_i = l_{oi}/l_i$ have been introduced. Now, in order to obtain the mapping (4.2), it remains only to substitute $\delta\hat{D}_o$ for δl_i and $l_i\delta\theta_i$.

In Figures 4.2 and 4.3, the i^{th} spring is shown to be connected to the moving body at pivot point C_i. When the moving body rotates $\delta\phi$ relative to the fixed body about an axis through P, the moving pivot point C_i displaces to the point C_i'. This displacement can be decomposed into two components: an infinitesimal displacement δl_i along the line $\$_i$ together with an infinitesimal displacement $l_i\delta\theta_i$ that is tangent to a circle of radius l_i centered at B_i. It should be clear from Figure 4.3 that

$$\delta l_i = p_i \, \delta\phi \quad \text{and} \quad l_i \delta\theta_i = q_i \, \delta\phi \, , \tag{4.10}$$

where p_i and q_i are respectively the perpendicular distances from P to the line $\$_i$ and from P to the line $\delta\$_i^*$, which is perpendicular to $\$_i$ at C_i. (The lines $\delta\$_i$ and $\delta\$_i^*$ are parallel, separated by the distance l_i.) The above perpendicular distances can be obtained as moments of the lines about P, which yields the coordinate expressions

$$p_i = \hat{s}_i^T \, \hat{S}_o \quad \text{and} \quad q_i = \delta\hat{s}_i^{*T} \, \hat{S}_o \, , \tag{4.11}$$

where $\delta\hat{s}_i^* = [-s_i, \, c_i; \, \delta r_i^*]^T$ $(\delta r_i^* = l_i + b_{xi} \, c_i + b_{yi} \, s_i)$ are the coordinates of the line $\delta\$_i^*$. Substituting (4.11) into (4.10) and substituting (4.5) into the result yields

$$\delta l_i = \hat{s}_i^T \, \delta\hat{D}_o \quad \text{and} \quad l_i \delta\theta_i = \delta\hat{s}_i^{*T} \, \delta\hat{D}_o \, . \tag{4.12}$$

Substituting (4.12) into (4.9) yields the mapping (4.2), where the stiffness matrix is given by

$$[K_o] = [j] \, [k_i] \, [j]^T + [\delta j] \, [k_i(1 - \rho_i)] \, [\delta j^*]^T, \tag{4.13}$$

where

$[k_i]$ and $[k_i(1 - \rho_i)]$ are 3x3 diagonal spring constant matrices,

the i^{th} column of the 3x3 $[j]$ is $\hat{s}_i$,

the i^{th} column of the 3x3 $[\delta j]$ is $\dfrac{\delta\hat{s}_i}{\delta\theta_i}$, and

the i^{th} column of the 3x3 $[\delta j^*]$ is $\delta\hat{s}_i^*$.

The stiffness matrix referenced to the fixed body is therefore expressed as the sum of two matrices: one that is symmetric, and one that is asymmetric for $\rho_i \neq 1$.

4.2 Moving-Body Reference Frame

Referring to the coupling shown in Figure 4.4, it is required to determine a mapping that relates the axis through point P of a $(-\delta\phi)$ rotation to a line $\$_b$ of a force (δf) increment in the static force applied to the moving body. In this section, this mapping is referenced to the moving body, which means that the two external static forces which keep the moving body in static equilibrium before and after the $(-\delta\phi)$ rotation are referenced to (or are drawn in) the moving body. The difference in these two static forces is the force increment that occurs along the line $\$_b$.

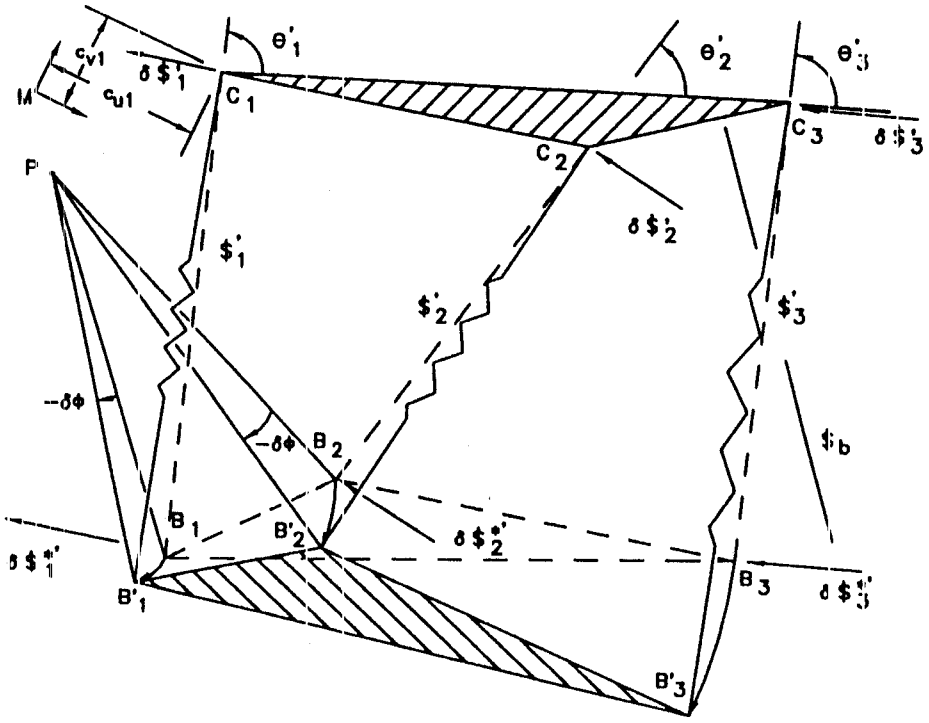

Figure 4.4 Motion of the Platform with respect to a Reference Frame in the Moving Body

Here, expressed in terms of an uv coordinate system that is located at some point M in the fixed body, this mapping is

$$\delta\hat{\mathrm{w}}_{\mathrm{m}} = [\mathrm{K_m}]\ (-\delta\hat{\mathrm{D}}_{\mathrm{m}})\ , \tag{4.14}$$

where the coordinates of the force increment are $\delta\hat{\mathrm{w}}_{\mathrm{m}} = [\delta \mathrm{F_u},\ \delta \mathrm{F_v};\ \delta m_{\mathrm{m}}]^{\mathrm{T}}$, the coordinates of the $(-\delta\phi)$ rotation are $\delta\hat{\mathrm{D}}_{\mathrm{m}} = [\delta u_{\mathrm{m}},\ \delta v_{\mathrm{m}};\ -\delta\phi]^{\mathrm{T}}$, and $[\mathrm{K_m}]$ is a 3x3 stiffness matrix. ($\delta\hat{\mathrm{D}}_{\mathrm{m}}$ expresses the displacement of the fixed body relative to the moving, and therefore $(-\delta\hat{\mathrm{D}}_{\mathrm{m}})$ expresses the displacement of the moving body relative to the fixed, which is required for the mapping.) Before the $(-\delta\phi)$ rotation, the static force applied to the moving body required to keep it in static equilibrium is given by the coordinates, $\hat{\mathrm{w}}_{\mathrm{m}} = [\mathrm{F_u},\ \mathrm{F_v};\ m_{\mathrm{m}}]^{\mathrm{T}}$, whereas after the $(-\delta\phi)$ rotation, the new static force is given by the coordinates $\hat{\mathrm{w}}^{+}_{\mathrm{m}} = [\mathrm{F}^{+}_{\mathrm{u}},\ \mathrm{F}^{+}_{\mathrm{v}};\ m^{+}_{\mathrm{m}}]^{\mathrm{T}}$. (Here, the three coordinates of a force denote the projections of the force onto the u and v axes and the moment of the force about the point M.) The coordinates of the force increment referenced to the moving body are then obtained from

$$\delta\hat{\mathrm{w}}_{\mathrm{m}} = \hat{\mathrm{w}}^{+}_{\mathrm{m}} - \hat{\mathrm{w}}_{\mathrm{m}}\ , \tag{4.15}$$

where $\delta \mathrm{F_u} = \mathrm{F}^{+}_{\mathrm{u}} - \mathrm{F_u}$, $\delta \mathrm{F_v} = \mathrm{F}^{+}_{\mathrm{v}} - \mathrm{F_v}$, and $\delta m_{\mathrm{m}} = m^{+}_{\mathrm{m}} - m_{\mathrm{m}}$.

The infinitesimal displacements δu_{m} and δv_{m} are of the point in the fixed body that is coincident with M, while the infinitesimal rotation $(-\delta\phi)$ denotes a change in orientation of the fixed body relative to the moving body. (The rotation about the axis through P is inverted from the previous section.) These three coordinates taken together form $\delta\hat{\mathrm{D}}_{\mathrm{m}}$, which locates an axis of rotation through the point P, whose coordinates u_{p} and v_{p} are obtained from

$$u_{\mathrm{p}} = -\delta v_{\mathrm{m}}/(-\delta\phi) \quad \text{and} \quad v_{\mathrm{p}} = \delta u_{\mathrm{m}}/(-\delta\phi)\ . \tag{4.16}$$

When the axis of rotation is quantified by the coordinates $\hat{S}_m = [v_p, -u_p; 1]^T$, then the $(-\delta\phi)$ rotation can be expressed as the scalar multiple

$$\delta\hat{D}_m = (-\delta\phi)\,\hat{S}_m\,, \tag{4.17}$$

which specify how the fixed body rotates relative to the moving one. The coordinates $(-\delta\hat{D}_m)$, on the other hand, specify how the moving body rotates relative to the fixed one. This latter rotation is the one that must be used in the stiffness mapping (4.14).

In order to derive the mapping of stiffness (4.14), it is necessary to first express the external static force applied to the moving platform as the resultant of the forces in the springs, f_1, f_2, and f_3:

$$\hat{w}_m = f_1\,\hat{s}'_1 + f_2\,\hat{s}'_2 + f_3\,\hat{s}'_3\,, \tag{4.18}$$

where $\hat{s}'_i = [c'_i, s'_i; r'_i]^T$ are the coordinates (direction cosines and perpendicular distance from M) of the line $\$'_i$ of the i^{th} spring. (Refer to Figure 4.4, $c'_i = \cos(\theta'_i)$, $s'_i = \sin(\theta'_i)$, and $r'_i = c_{ui}\,s'_i - c_{vi}\,c'_i$, where c_{ui} and c_{vi} are the coordinates of the moving pivot point C_i.) Substituting into (4.18) the relations $f_i = k_i(l_i - l_{oi})$, where k_i and $(l_i - l_{oi})$ are respectively the spring constant and difference between the current and free lengths of the i^{th} spring, yields

$$\hat{w}_m = k_1(l_1 - l_{o1})\,\hat{s}'_1 + k_2(l_2 - l_{o2})\,\hat{s}'_2 + k_3(l_3 - l_{o3})\,\hat{s}'_3\,. \tag{4.19}$$

Successive applications of (4.19), which yields $\hat{w}_m$ and $\hat{w}_m^+$, could provide the coordinates of force increment. However, in order to obtain the mapping (4.14), it is desirable to differentiate (4.19), which yields

$$\delta\hat{w}_m = k_1\,\delta l_1\,\hat{s}'_1 + k_2\,\delta l_2\,\hat{s}'_2 + k_3\,\delta l_3\,\hat{s}'_3 +$$

$$k_1(l_1 - l_{o1})\,\frac{\delta\hat{s}'_1}{\delta\theta'_1}\,\delta\theta'_1 + k_2(l_2 - l_{o2})\,\frac{\delta\hat{s}'_2}{\delta\theta'_2}\,\delta\theta'_2 + k_3(l_3 - l_{o3})\,\frac{\delta\hat{s}'_3}{\delta\theta'_3}\,\delta\theta'_3\,. \tag{4.20}$$

The coordinates, $\frac{\delta \hat{\mathrm{s}}_{\mathrm{i}}'}{\delta \theta_{\mathrm{i}}'} = [-s_{\mathrm{i}}', c_{\mathrm{i}}'; \delta r_{\mathrm{i}}']^{\mathrm{T}}$ (where $\delta r_{\mathrm{i}}' = \mathrm{c}_{\mathrm{ui}}\, c_{\mathrm{i}}' + \mathrm{c}_{\mathrm{vi}}\, s_{\mathrm{i}}'$), locate a line $\delta \$_{\mathrm{i}}'$ that is perpendicular to the line of the spring $\$_{\mathrm{i}}'$ at that line's moving pivot point C_{i}, and therefore, the line $\delta \$_{\mathrm{i}}'$ is defined as the geometric derivative of $\$_{\mathrm{i}}'$ referenced to the moving body (see Figure 4.4). An equivalent form of (4.20) is

$$\delta \hat{\mathrm{w}}_{\mathrm{m}} = k_1\, \delta l_1\, \hat{\mathrm{s}}_1' + k_2\, \delta l_2\, \hat{\mathrm{s}}_2' + k_3\, \delta l_3\, \hat{\mathrm{s}}_3' +$$

$$k_1(1-\rho_1)\, \frac{\delta \hat{\mathrm{s}}_1'}{\delta \theta_1'}\, l_1\, \delta \theta_1' + k_2(1-\rho_2)\, \frac{\delta \hat{\mathrm{s}}_2'}{\delta \theta_2'}\, l_2\, \delta \theta_2' + k_3(1-\rho_3)\, \frac{\delta \hat{\mathrm{s}}_3'}{\delta \theta_3'}\, l_3\, \delta \theta_3', \quad (4.21)$$

where the parameters, $\rho_{\mathrm{i}} = l_{\mathrm{ci}}/l_{\mathrm{i}}$ have been introduced. Now, in order to obtain the mapping (4.14), it remains only to substitute $\delta \hat{\mathrm{D}}_{\mathrm{m}}$ for δl_{i} and $l_{\mathrm{i}} \delta \theta_{\mathrm{i}}'$.

In Figure 4.4, the i^{th} spring is shown to be connected to the fixed body at pivot point B_{i}. When the fixed body rotates $(-\delta\phi)$ relative to the moving body about an axis through P, the fixed pivot point B_{i} displaces to the point B_{i}'. This displacement can be decomposed into two components: an infinitesimal displacement δl_{i} along the line $\$_{\mathrm{i}}'$ together with an infinitesimal displacement $l_{\mathrm{i}} \delta \theta_{\mathrm{i}}'$ that is tangent to a circle of radius l_{i} centered at C_{i}. In analogy with Figure 4.3, it should be clear that

$$\delta l_{\mathrm{i}} = p_{\mathrm{i}}\, \delta\phi \quad \text{and} \quad l_{\mathrm{i}} \delta \theta_{\mathrm{i}}' = q_{\mathrm{i}}\, \delta\phi\,, \quad (4.22)$$

where p_{i} and q_{i} are respectively the perpendicular distances from P to the line $\$_{\mathrm{i}}'$ and from P to the line $\delta \$_{\mathrm{i}}^{*\prime}$, which is perpendicular to $\$_{\mathrm{i}}'$ at B_{i}. (The lines $\delta \$_{\mathrm{i}}'$ and $\delta \$_{\mathrm{i}}^{*\prime}$ are parallel, separated by the distance l_{i}.) The above perpendicular distances can be obtained as moments of the lines about P, which yields the coordinate expressions

$$p_{\mathrm{i}} = \hat{\mathrm{s}}_{\mathrm{i}}'^{\mathrm{T}}\, \hat{\mathrm{S}}_{\mathrm{m}} \text{ and } q_{\mathrm{i}} = \delta \hat{\mathrm{s}}_{\mathrm{i}}^{*\prime\mathrm{T}}\, \hat{\mathrm{S}}_{\mathrm{m}}\,, \quad (4.23)$$

where $\delta \hat{\mathrm{s}}_{\mathrm{i}}^{*\prime} = [-s_{\mathrm{i}}', c_{\mathrm{i}}'; \delta r_{\mathrm{i}}^{*\prime}]^{\mathrm{T}}$ $(\delta r_{\mathrm{i}}^{*\prime} = l_{\mathrm{i}} + \mathrm{c}_{\mathrm{ui}}\, c_{\mathrm{i}}' + \mathrm{c}_{\mathrm{vi}}\, s_{\mathrm{i}}')$ are the coordinates of the line $\delta \$_{\mathrm{i}}^{*\prime}$. Substituting (4.23) into (4.22) and using (4.17) in the result yields

$$\delta l'_i = \hat{s}'^{T}_i \, (-\delta \hat{D}_m) \text{ and } l_i \delta\theta'_i = \delta \hat{s}^{*\prime T}_i \, (-\delta \hat{D}_m) \, . \tag{4.24}$$

Substituting (4.24) into (4.21) yields the mapping (4.14), where the stiffness matrix is given by

$$[K_m] = [j'] \, [k_i] \, [j']^T + [\delta j'] \, [k_i(1-\rho_i)] \, [\delta j^{*\prime}]^T, \tag{4.25}$$

where

$[k_i]$ and $[k_i(1-\rho_i)]$ are 3x3 diagonal spring constant matrices,

the i^{th} column of the 3x3 $[j']$ is $\hat{s}'_i$,

the i^{th} column of the 3x3 $[\delta j']$ is $\dfrac{\delta \hat{s}'_i}{\delta \theta'_i}$, and

the i^{th} column of the 3x3 $[\delta j^{*\prime}]$ is $\delta \hat{s}^{*\prime}_i$.

The stiffness matrix referenced to the moving body is therefore expressed as the sum of two matrices: one that is symmetric, and a second that is asymmetric for $\rho_i \neq 1$.

The results obtained in this section can be compared to those obtained in Section 4.1 by introducing the transformations that relate line coordinates expressed in the uv coordinate system at M to line coordinates expressed in the xy coordinate system at O:

$$\hat{s}_i = [e] \, \hat{s}'_i, \quad \frac{\delta \hat{s}_i}{\delta \theta_i} = [e] \, \delta \hat{s}^{*\prime}_i, \quad \delta \hat{s}^{*}_i = [e] \, \frac{\delta \hat{s}'_i}{\delta \theta_i}, \text{ and } \delta \hat{D}_o = [E] \, (-\delta \hat{D}_m), \tag{4.26}$$

where

$$[e] = \begin{bmatrix} c_\phi & -s_\phi & 0 \\ s_\phi & c_\phi & 0 \\ x_m \, s_\phi - y_m \, c_\phi & x_m \, c_\phi + y_m \, s_\phi & 1 \end{bmatrix},$$

And where $[E] = [e]^{-T}$. The angle ϕ ($c_\phi = \cos(\phi)$ and $s_\phi = \sin(\phi)$) is used to measure the orientation of the u-axis of the uv coordinate system relative to the

x-axis of the xy coordinate system, and the coordinates x_m and y_m locate the point M in terms of the xy coordinate system at O. The transformations (4.26) also provide $[j] = [e][j']$, $[\delta j] = [e][\delta j^{*\prime}]$, and $[\delta j^*] = [e][\delta j']$. An additional transformation is also required,

$$\delta\hat{w}_o = [e]\ \delta\hat{w}'_o\ , \tag{4.27}$$

which relates the xy- and uv-based coordinates of the fixed-body-referenced force increment. (The sets of coordinates, $\delta\hat{w}_o$ and $\delta\hat{w}'_o$, are used to locate the line $\$_a$ of the fixed-body-referenced force increment, while the set of uv-based coordinates $\delta\hat{w}_m$ is used to locate the line $\$_b$ of the moving-body-referenced force increment.)

Substituting the above transformations into (4.2) and inverting [e] yields the fixed-body-referenced stiffness mapping in terms of the moving body uv coordinate system at M:

$$\delta\hat{w}'_o = [e]^{-1}[K_o]\ [E]\ (-\delta\hat{D}_m)\ . \tag{4.28}$$

Substituting the transformations (4.26) into (4.13) yields

$$[K_o] = [e]\ [j']\ [k_i]\ [j']^T\ [e]^T + [e]\ [\delta j'^*]\ [k_i(1-\rho_i)]\ [\delta j']^T\ [e]^T. \tag{4.29}$$

Substituting (4.29) into (4.28), simplifying, and using the substitution $[E] = [e]^{-T}$ gives

$$\delta\hat{w}'_o = [K'_o]\ (-\delta\hat{D}_m)\ , \tag{4.30}$$

where

$$[K'_o] = [j']\ [k_i]\ [j']^T + [\delta j^{*\prime}]\ [k_i(1-\rho_i)]\ [\delta j']^T. \tag{4.31}$$

A comparison of the stiffness matrices (4.31) and (4.25) shows conclusively that

$$[K_m] = [K'_o]^T, \tag{4.32}$$

which is indicative of the fact that the roles of the derivative lines ($\delta\$$) and the kinematic substitution lines ($\delta\$^*$) are reversed in the two mappings referenced to

the fixed and moving bodies. This can be visualized by comparing Figures 4.2 and 4.4. The lines $\$_i$ and $\$'_i$ are the same and share the same role of locating the i^{th} spring line. On the other hand, $\delta\$_i$ and $\delta\$^{*\prime}_i$ are the same lines, but they play different roles. (The same can be said of the pair of lines $\delta\$^{*}_i$ and $\delta\$'_i$.)

While the relative motion between the moving and fixed bodies is the same, it is clear from (4.32) that the fixed-body-referenced and moving-body-referenced force increments are not the same. Due to the nature of the asymmetries in $[K'_O]$ and $[K_{rn}]$, the two force increments will be parallel acting along the parallel lines $\$_a$ and $\$_b$ and having the uv coordinates (referenced to M) of respectively, $\delta\hat{w}'_O$ and $\delta\hat{w}_{rn}$.

4.3 Symmetric-Body Stiffness Mapping

In this section, a stiffness mapping is derived which is always symmetric, regardless of the degree of loading of the coupling. With regard to the displacement-rotation input ($\delta\hat{D}_q$) and the force-increment output ($\delta\hat{w}_q$), the mapping obtained here

$$\delta\hat{w}_q = [K_q]\ \delta\hat{D}_q \tag{4.33}$$

agrees in philosophy with those typically found in the literature. It is customary to express the potential energy of the system as a function of the displacement (x_q, y_q) of a pre-selected point Q in the moving body and the rotation (ϕ) of the moving body about an axis through Q. Often, one then finds the stiffness matrix to be the Hessian of the resulting potential function similar to the mapping for the two-spring coupling derived in Chapter 2.

Although the three coordinates (x_q, y_q, ϕ) are measured relative to the

fixed body's xy coordinate system located at O, it is of paramount importance to realize that the body of reference (to which the force increment $\delta\hat{w}_q$ is referenced) is not the fixed body. It is in fact a body that undergoes rectilinear motion with respect to the fixed body, and it is a body that is hinged to the moving body at Q (see Figure 4.5). In other words, both the fixed and moving bodies displace relative to the frame of reference of this section. Specifically, while keeping the same orientation with respect to the fixed body, this body of reference purely translates with the point Q of the moving body. Such a body of reference is referred to here as a "symmetric body of reference."

This means that the two external forces which keep the moving body in static equilibrium before and after the $\delta\phi$ rotation are referenced to (or are drawn in) the symmetric body of reference. The difference in these two static forces is the force increment that occurs along a line $\$_C$.

Referring to Figure 4.5, it is required in this section to determine a mapping that relates the axis through point P of a $\delta\phi$ rotation to a line $\$_C$ to a force (δf) increment in the static force applied to the moving body. Here, the mapping is (4.33), which is given in terms of a xy coordinate system located at point Q. Then, the coordinates of the force increment are $\delta\hat{w}_q = [\delta F_x, \delta F_y; \delta m_q]^T$, the coordinates of the $\delta\phi$ rotation are $\delta\hat{D}_q = [\delta x_q, \delta y_q; \delta\phi]^T$, and $[K_q]$ is the symmetric 3x3 stiffness matrix. Before the $\delta\phi$ rotation, the static force applied to the moving body required to keep it in static equilibrium is given by the coordinates, $\hat{w}_q = [F_x, F_y; m_q]^T$, whereas after the $\delta\phi$ rotation, the new static force is given by the coordinates $\hat{w}_q^+ = [F_x^+, F_y^+; m_q^+]^T$. (The three coordinates of a force denote the projections of the force onto the x and y axes

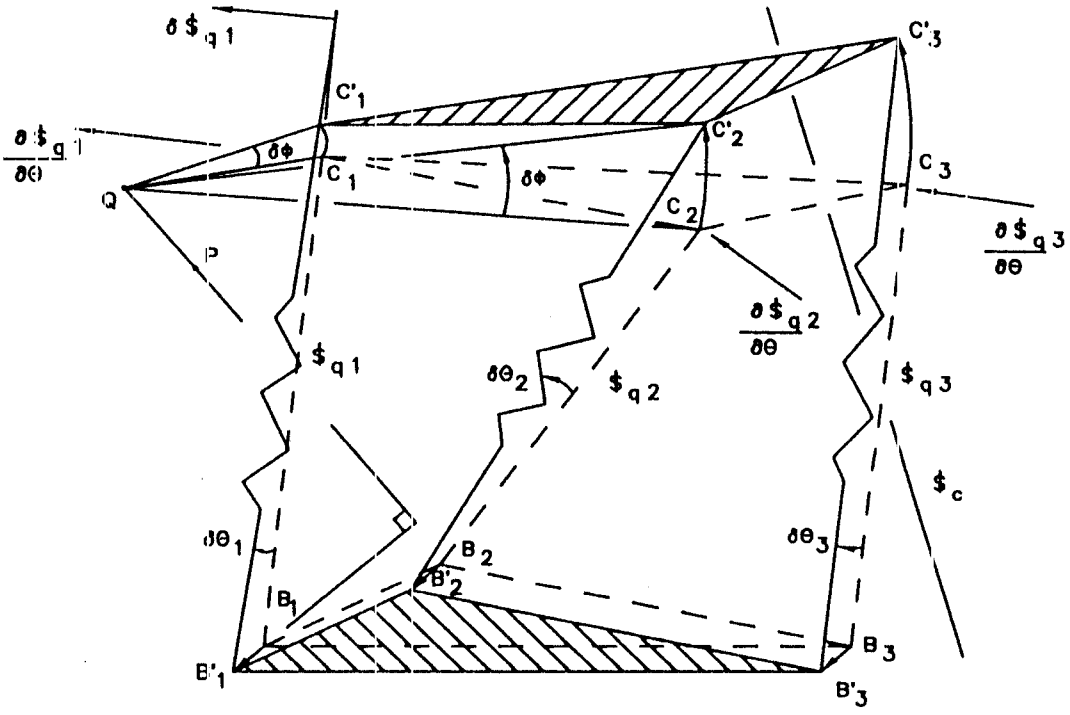

Figure 4.5 Motion of the Platform with respect to a Reference Frame Producing a Symmetric Mapping Matrix

and the moment of the force about the point Q.) The coordinates of the force increment referenced to the symmetric body are then obtained from

$$\delta\hat{w}_q = \hat{w}_q^+ - \hat{w}_q \,, \tag{4.34}$$

where $\delta F_x = F_x^+ - F_x$, $\delta F_y = F_y^+ - F_y$, and $\delta m_q = m_q^+ - m_q$.

The infinitesimal displacements δx_q and δy_q denote how the point in the moving body that is coincident with Q displaces relative to the fixed body. The infinitesimal rotation $\delta\phi$ denotes a change in orientation of the moving body relative to the fixed body. These three coordinates taken together form $\delta\hat{D}_q$, which locates an axis of rotation through the point P, whose coordinates x'_p and

y'_p (relative to Q) are obtained from

$$x'_p = -\delta y_q/\delta\phi \quad \text{and} \quad y'_p = \delta x_q/\delta\phi \,. \tag{4.35}$$

When the axis of rotation is quantified by the coordinates $\hat{S}_q = [y'_p,\ -x'_p;\ 1]^T$, then the $\delta\phi$ rotation can be expressed as the scalar multiple

$$\delta\hat{D}_q = \delta\phi\ \hat{S}_q \,, \tag{4.36}$$

which specifies (in terms of the xy coordinate system at Q) how the moving body rotates relative to the fixed one. As a point of reference, it is noted that the moving body rotates $\delta\hat{D}_t = [0,\ 0;\ \delta\phi]^T$ relative to the symmetric body, while the fixed body displaces $\delta\hat{D}_b = \delta\hat{D}_t - \delta\hat{D}_q = [-\delta x_q,\ -\delta y_q;\ 0]^T$ relative to the symmetric one.

In order to derive the mapping of stiffness (4.33), it is necessary to first express the external static force applied to the moving platform as the resultant of the forces in the springs, f_1, f_2, and f_3:

$$\hat{w}_q = f_1\ \hat{s}_{q1} + f_2\ \hat{s}_{q2} + f_3\ \hat{s}_{q3} \,, \tag{4.37}$$

where $\hat{s}_{qi} = [c_i,\ s_i;\ r_{qi}]^T$ are the coordinates (direction cosines and perpendicular distance from Q) of the line $\$_{qi}$ of the i^{th} spring. For convenience, the point chosen to be Q is point M of section 4.1. Then, $c_i = \cos(\theta_i)$, $s_i = \sin(\theta_i)$, and

$$r_{qi} = c_{ui}\ s_{i\phi} - c_{vi}\ c_{i\phi} \,, \tag{4.38}$$

where c_{ui} and c_{vi} are the uv-based coordinates of the moving pivot points of section 4.1, where ϕ is again used to measure the angle between the u-axis and the x-axis, and where $s_{i\phi} = \sin(\theta_i - \phi)$ and $c_{i\phi} = \cos(\theta_i - \phi)$. Substituting into (4.37) the relations $f_i = k_i(l_i - l_{oi})$, where k_i and $(l_i - l_{oi})$ are respectively the spring constant and difference between the current and free lengths of the i^{th} spring, yields

$$\hat{w}_q = k_1(l_1 - l_{o1})\ \hat{s}_{q1} + k_2(l_2 - l_{o2})\ \hat{s}_{q2} + k_3(l_3 - l_{o3})\ \hat{s}_{q3} \,. \tag{4.39}$$

Successive applications of (4.39), which yields $\hat{w}_q$ and $\hat{w}_q^+$, could provide the coordinates of force increment. However, in order to obtain the mapping (4.33), it is desirable to differentiate (4.39), which yields

$$\delta\hat{w}_q = k_1\,\delta l_1\,\hat{s}_{q1} + k_2\,\delta l_2\,\hat{s}_{q2} + k_3\,\delta l_3\,\hat{s}_{q3} +$$

$$k_1(l_1 - l_{o1})\,\frac{\partial\hat{s}_{q1}}{\partial\theta_1}\,\delta\theta_1 + k_2(l_2 - l_{o2})\,\frac{\partial\hat{s}_{q2}}{\partial\theta_2}\,\delta\theta_2 + k_3(l_3 - l_{o3})\,\frac{\partial\hat{s}_{q3}}{\partial\theta_3}\,\delta\theta_3 +$$

$$k_1(l_1 - l_{o1})\,\frac{\partial\hat{s}_{q1}}{\partial\phi}\,\delta\phi + k_2(l_2 - l_{o2})\,\frac{\partial\hat{s}_{q2}}{\partial\phi}\,\delta\phi + k_3(l_3 - l_{o3})\,\frac{\partial\hat{s}_{q3}}{\partial\phi}\,\delta\phi. \quad (4.40)$$

The partial notation must be used here because a stationary pivot point in this reference frame cannot be found and thus the coordinates $\hat{s}_{qi}$ must be located using two variables, θ_i and ϕ. Therefore, the coordinates $\delta\hat{s}_{qi}$ of the line $\delta\$_{qi}$ that is the total derivative of $\$_{qi}$ (with respect to the symmetric body) are

$$\delta\hat{s}_{qi} = \frac{\partial\hat{s}_{qi}}{\partial\theta_i}\,\delta\theta_i + \frac{\partial\hat{s}_{qi}}{\partial\phi}\,\delta\phi\,, \quad (4.41)$$

where the coordinates, $\frac{\partial\hat{s}_{qi}}{\partial\theta_i} = [-s_i,\, c_i;\, \delta r_{qi}]^T$ (where $\delta r_{qi} = c_{ui}\,c_{i\phi} + c_{vi}\,s_{i\phi}$), locate a line $\frac{\partial\$_{qi}}{\partial\theta_i}$ that is perpendicular to the line of the spring $\$_{qi}$ at that line's moving pivot point C_i, and where, as in (4.40), $\frac{\partial\hat{s}_{qi}}{\partial\phi} = [0,\, 0;\, -\delta r_{qi}]^T$. (Refer to Figure 4.5.) An equivalent form of (4.40) is

$$\delta\hat{w}_q = k_1\,\delta l_1\,\hat{s}_{q1} + k_2\,\delta l_2\,\hat{s}_{q2} + k_3\,\delta l_3\,\hat{s}_{q3} +$$

$$k_1(1-\rho_1)\,\frac{\partial \widehat{s}_{q1}}{\partial \theta_1}\,l_1\,\delta\theta_1 + k_2(1-\rho_2)\,\frac{\partial \widehat{s}_{q2}}{\partial \theta_2}\,l_2\,\delta\theta_2 +$$

$$k_3(1-\rho_3)\,\frac{\partial \widehat{s}_{q3}}{\partial \theta_3}\,l_3\,\delta\theta_3 + k_1(1-\rho_1)\,l_1\,\frac{\partial \widehat{s}_{q1}}{\partial \phi}\,\delta\phi +$$

$$k_2(1-\rho_2)\,l_2\,\frac{\partial \widehat{s}_{q2}}{\partial \phi}\,\delta\phi + k_3(1-\rho_3)\,l_3\,\frac{\partial \widehat{s}_{q3}}{\partial \phi}\,\delta\phi\,. \qquad (4.42)$$

where the parameters, $\rho_i = l_{oi}/l_i$ have been introduced. Now, in order to obtain the mapping (4.33), it remains only to substitute $\delta\widehat{D}_q$ for δl_i, $l_i\delta\theta_i$, and $\delta\phi$.

In Figure 4.3, the i^{th} spring was shown to be connected to the moving body at pivot point C_i and to the fixed body at B_i. (This figure also applies in this section for the generation of the δl_i and $l_i\,\delta\theta_i$ substitutions, where $\$_i$ corresponds here to $\$_{qi}$.) When the moving body rotates $\delta\phi$ relative to the fixed body about an axis through P, the moving pivot point C_i displaces to the point C_i'. This displacement can again be decomposed into two components: an infinitesimal displacement δl_i along the line $\$_i$ together with an infinitesimal displacement $l_i\delta\theta_i$ that is tangent to a circle of radius l_i centered at B_i. It should be clear from Figure 4.3 that

$$\delta l_i = p_i\,\delta\phi \quad \text{and} \quad l_i\delta\theta_i = q_i\,\delta\phi\,, \qquad (4.43)$$

where p_i and q_i are respectively the perpendicular distances from P to the line $\$_i$ and from P to the line $\delta\$_i^*$, which is perpendicular to $\$_i$ at C_i. The line $\delta\$_i^*$ of Figure 4.3 corresponds to the line $\dfrac{\partial \$_{qi}}{\partial \theta_i}$ of this section, and therefore, the above perpendicular distances can be obtained as moments of the lines $\$_{qi}$ and $\dfrac{\partial \$_{qi}}{\partial \theta_i}$ about P, which yields the coordinate expressions

$$p_i = (\widehat{s}_{qi})^T\,\widehat{S}_q \quad \text{and} \quad q_i = \left(\frac{\partial \widehat{s}_{qi}}{\partial \theta_i}\right)^T \widehat{S}_q\,. \qquad (4.44)$$

Substituting (4.44) into (4.43) and substituting (4.36) into the result yields

$$\delta l_i = (\hat{s}_{qi})^T \delta \hat{D}_q \text{ and } l_i \delta\theta_i = \left(\frac{\partial \hat{s}_{qi}}{\partial \theta_i}\right)^T \delta \hat{D}_q \,. \tag{4.45}$$

Substituting (4.45) into (4.42) yields the mapping (4.33), where the stiffness matrix is given by

$$[K_q] = [j_q]\,[k_i]\,[j_q]^T + [\partial j_q]\,[k_i(1-\rho_i)]\,[\partial j_q]^T + [\Phi]\,, \tag{4.46}$$

where

$[k_i]$ and $[k_i(1-\rho_i)]$ are 3x3 diagonal spring constant matrices,

the i^{th} column of the 3x3 $[j_q]$ is $\hat{s}_{qi}$,

the i^{th} column of the 3x3 $[\partial j_q]$ is $\frac{\partial \hat{s}_i}{\partial \theta_i}$, and

the 3x3 matrix $[\Phi]$ has zeros except for the 33 entry which is

$$-k_1(1-\rho_1)\,l_1\,\delta r_{q1} \; -k_2(1-\rho_2)\,l_2\,\delta r_{q2} \; -k_3(1-\rho_3)\,l_3\,\delta r_{q3}.$$

The stiffness matrix referenced to the symmetric body is therefore expressed as the sum of three matrices, all of which are symmetric regardless of ρ_i. The nature of the asymmetries in $[K_o]$ of Section 4.1 and $[K_m]$ of Section 4.2 yields that the fixed-body-referenced force increment line $\$_a$, the moving-body-referenced force increment line $\$_b$, and the symmetric-body-referenced force increment line $\$_c$ are all parallel.

It is important to realize that the choice of a symmetric body of reference is not a practical one. Analytically, it yields the apparently simple symmetric mapping, but the matrix $[K_q]$ cannot be directly used in a control algorithm such as that detailed in [3] and [5]. This is because a force/torque sensor used to sense the actual static force applied to the moving body is mounted either on the moving body or the fixed one. (It does not translate with the moving one, while keeping constant orientation with the fixed body.)

4.4 Static Force Loci

While the preceding sections have demonstrated that the mapping of stiffness is dependent on the chosen frame of reference, this section shows, in both the fixed and moving bodies, the line loci of the external static force which must be applied to the moving body to keep it in static equilibrium. A line locus is a curve generated by the envelope of a line moving in a defined frame of reference (a plane or a lamina). These static force loci drawn in the fixed and moving bodies form a static analogy to the fixed and moving centrodes, which are their kinematic counterparts.

Again we will use the planar compliant coupling of Figure 4.1. The line \$ is the line along which the external static force must be applied to keep the moving body in static equilibrium while the coupling is in this particular configuration. Figure 4.6 illustrates a candidate motion of the moving body and shows how the line \$ creates the the *fixed-body static force locus*. Figure 4.7, on the other hand, illustrates only the moving body and shows the *moving-body static force locus* that was created by \$.

Figure 4.8 shows several intermediate configurations of this same motion with the fixed-body (F) and moving-body (M) static force loci. At each instant, both of the loci are tangent to \$, which carries the current external static force, but they are tangent to \$ at different points. This substantiates the fact that the derivatives are frame-of-reference dependent and inherently explains the differences in the stiffness mapping matrices derived in the previous section. Equation (4.3) has analytically demonstrated that the fixed-body-referenced force

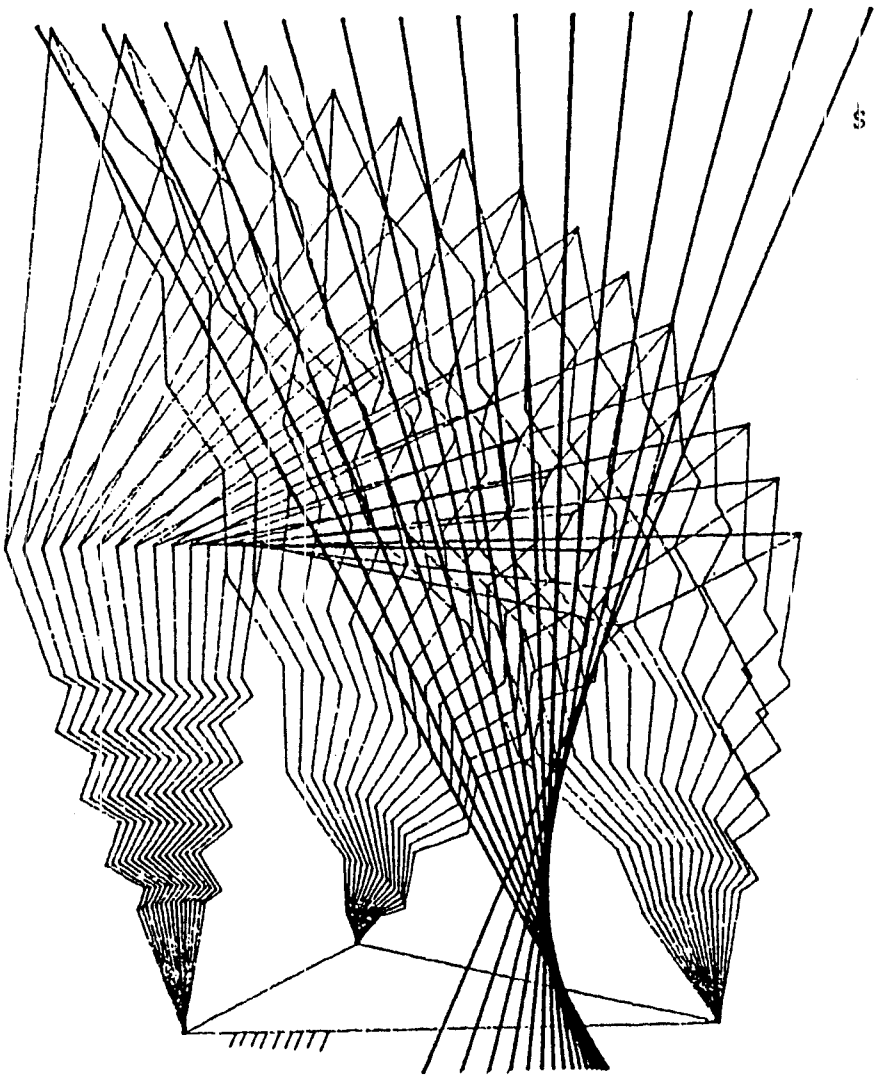

Figure 4.6 Fixed-Body Static Force Locus

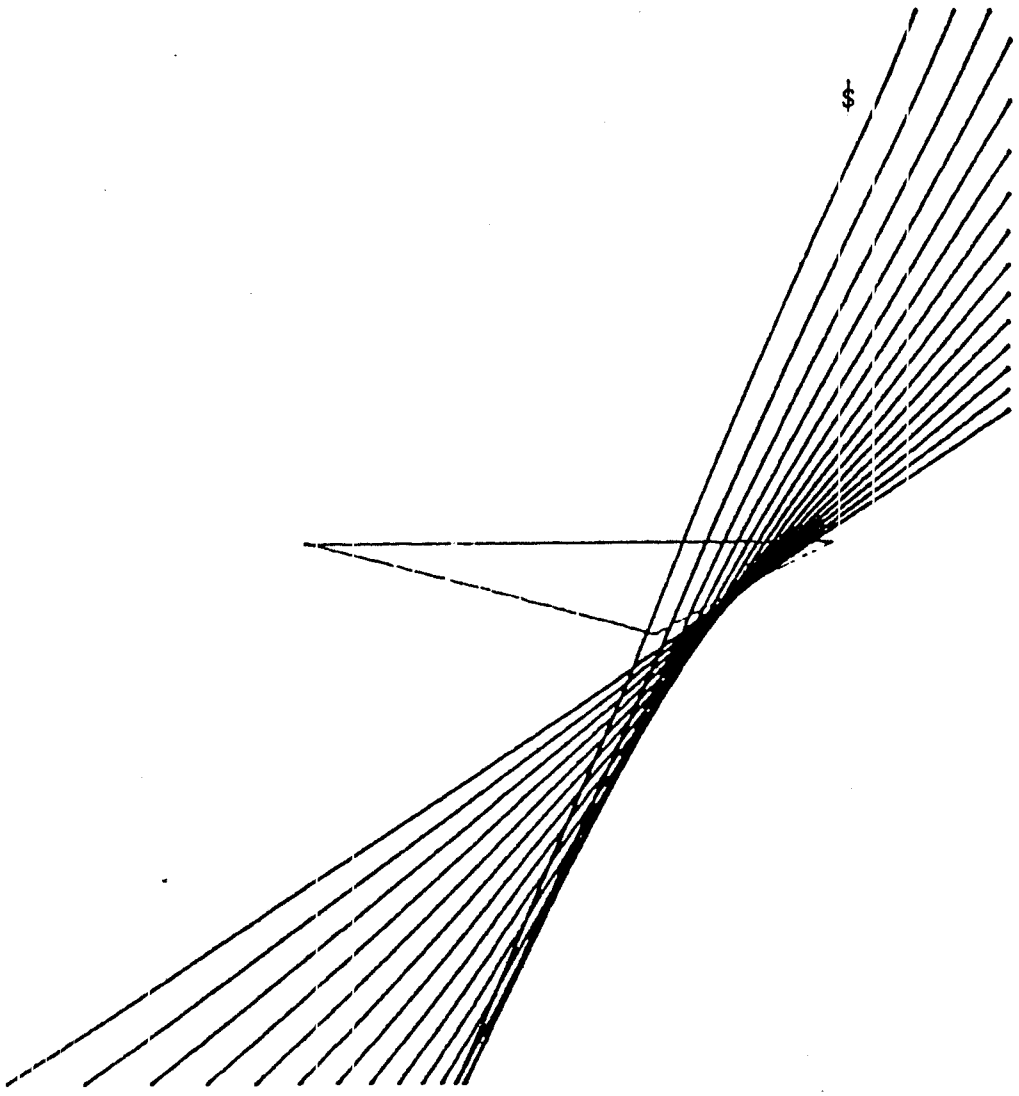

Figure 4.7 Moving-Body Static Force Locus

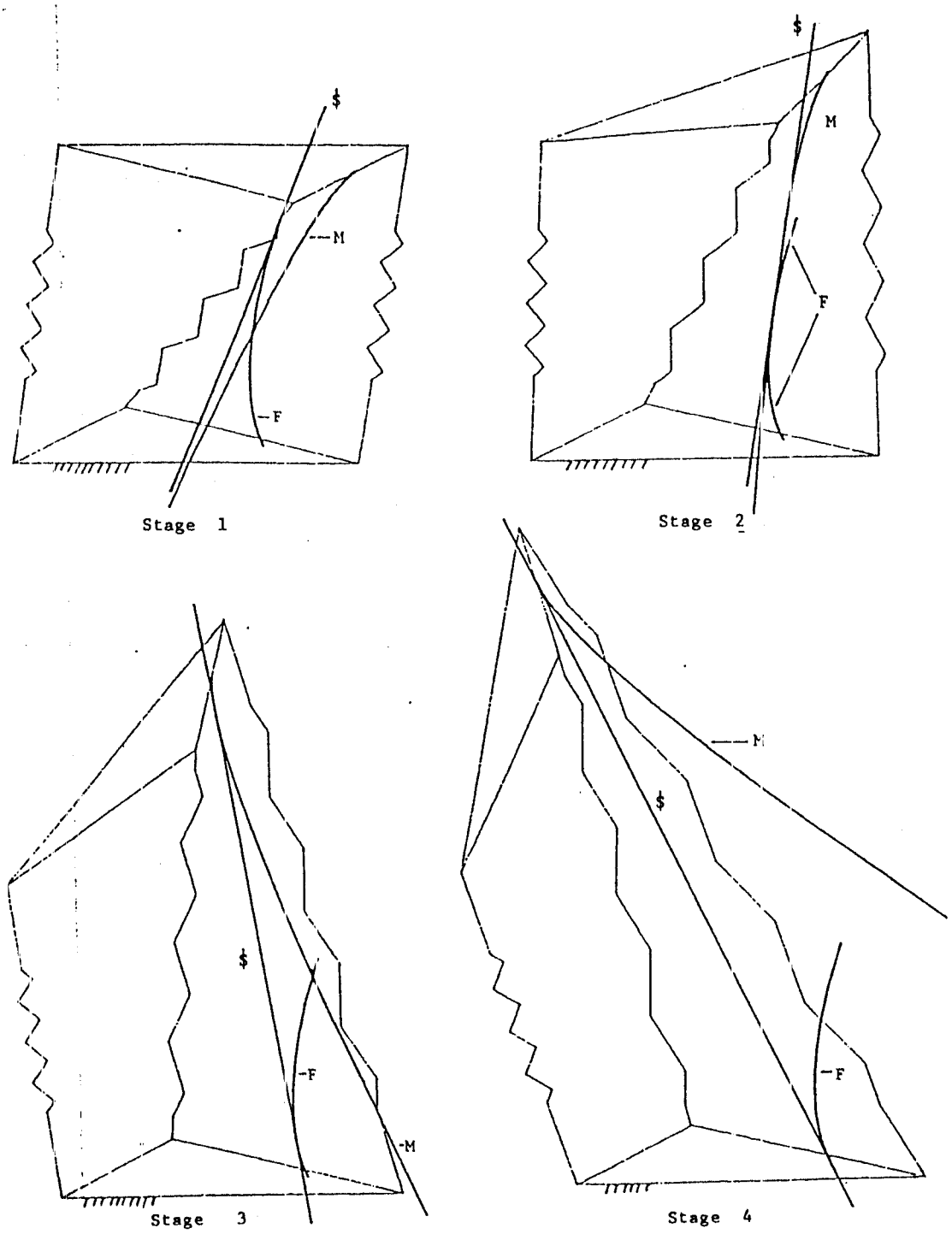

Figure 4.8 Intermediate Configurations of the Fixed-Body and Moving-Body Static Force Locus

increment is the difference between the external static forces before and after the $\delta\phi$ rotation, both drawn in the fixed body. Geometrically, this means that the three lines in the fixed body consisting of the current static force, the next static force, and the fixed-body-referenced force increment all pass through the same point, which must be the point of tangency of \$ on the fixed-body static force locus. Likewise, Equation (4.15) has analytically demonstrated that the moving-body-referenced force increment is the difference between the external static forces before and after the $\delta\phi$ rotation, both drawn now in the moving body. Geometrically, this likewise means that the three lines must pass through the same point, but here, it is the point of tangency of \$ on the moving-body static force locus. It should be noted that in the example shown in Figure 4.8 the fixed and moving points of tangency have differing relative distances along \$ throughout the motion, which means that these two curves roll with slip on \$.

CHAPTER 5
CONCLUSIONS

A knowledge of the behavior of compliant couplings such as the two presented in this thesis is essential for the improvement of modern force-control techniques. Advanced research in the area of simultaneous position and force control of a robotic end-effector, which was the impetus for this author's work, and in the area of active suspension systems, which is currently a hot topic of research, will rely more and more on the basic understanding of the compliant couplings.

5.1 The Planar Two-Spring Coupling

In Chapter 3, a novel closed-form inverse analysis of the planar two-spring coupling was presented. This analysis not only produced the exact number of assembly configurations for a desired resultant, but also provided a simple tool for analyzing the motion of the movable pivot for all six roots as the desired applied load changed. In the example of 3.3, the behavior exhibited by the mechanism was unexpected. The motion of movable pivot P described by the curves CF3, CF4, and CF6 of Figure 3.4 was away from the direction of applied force. This phenomena was surprising, and intuitively it appeared to flag an instability. However, discussion on this subject since its original presentation [15] has revealed that mechanisms which exhibit this behavior have been seen before, and often they are used to compensate the action of regular springs. Their action

has been compared with that of a spring with negative stiffness. Eijk and Dijksman[19] have cataloged occurrences of negative stiffness in several mechanisms including the planar two-spring coupling (see also Eijk[20]).

Another interesting result of the inverse analysis example was the apparent merger of the traces CF2 and CF6 at point M in Figure 3.4. If the force were increased when the system was in this configuration, two of the roots to the inverse solution went complex, and the author stated the system would behave unpredictably. Additional discussion on this behavior revealed it to be indicative of a "catastrophe." A catastrophe occurs when there is a loss in continuity of a smooth and slow response to a smooth and slow input. Zeeman[21] has analyzed several catastrophe machines which exhibit a "jump" to a new configuration when a predicted critical point is reached. The analysis of this mechanism as a catastrophe machine is an area of further research which should be pursued.

Other areas of further research include the development of springs which can achieve negative lengths and the development of an inverse solution for a spatial three-spring coupling. Research on the inverse solution to this tetrahedron problem is novel and may well have a major impact. It can be deduced that the problem would exhibit similar catastrophic behavior. Initial attempts have so far been unsuccessful at solving this problem.

5.2 The Planar Three-Spring Coupling

In Chapter 4, the stiffness mapping of a planar three-spring coupling was analyzed from three reference frames: the fixed-body of the coupling, the moving body of the coupling, and a body which always yielded a symmetric mapping matrix. The impetus was to justify asymmetric matrices previously reported by

Griffis and Duffy[5] and Griffis[3]. The fixed body and moving body stiffness mapping were indeed found to be asymmetric, and one was the transpose of the other. These mappings are essential for control of the coupling since it is to these two frames a force/torque sensor can be mounted to sense the actual static force applied to the moving body. The third reference frame yielded an analytically simple symmetric mapping which was identical to the Hessian obtained by the second differentials of the elastic potential energy function reported by Loncaric[12]. However, this simple symmetric mapping cannot be used in current control algorithms.

The results derived in this thesis for the simple planar coupling can intuitively be extended to the simple six-spring spatial coupling. At this stage however these results are theoretical. Griffis[3] achieved successful results using a coupling for which the mapping was experimentally derived. However, no results have been obtained using a coupling for which the mapping was obtained purely from the geometry of the coupling and the spring characteristics as outlined in this thesis. Initial attempts at manufacturing the planar coupling described in this thesis were unsuccessful due to poor test results on the spring to be used in the experimental analysis. The assumption of frictionless and massless springs has not yet been overcome. The development of a working experimental coupling is a subject of further research.

REFERENCES

1. Vanderplaats, G., *Numerical Optimization Techniques for Engineering Design:With Applications,* McGraw Hill, New York, 1984.

2. Seireg, A., *Mechanical System Analysis,* International Textbook, Scranton, Pennsylvania, 1969.

3. Griffis, M., 1991, "Kinestatic Control: A Novel Theory for Simultaneously Regulating Force and Displacement," Ph.D. Dissertation, University of Florida.

4. Griffis, M., 1992, "Comparing Structures of Stiffness Matrices Using Invariants," Presented at the VIII CISM-IFToMM Symposium "Ro. Man. Sy '92", Udine, Italy..

5. Griffis, M., and Duffy, J., 1991, "Kinestatic Control: A Novel Theory for Simultaneously Regulating Force and Displacement," ASME Journal of Mechanical Design, Vol. 113.

6. Dimentberg, F., 1967, "The Screw Calculus and its Applications in Mechanics," Translated and Published by The Foreign Technology Division (United States Department of Commerce), Washington D.C.

7. Salisbury, K., 1980, "Active Stiffness Control of a Manipulator in Cartesian Coordinates," Proc. IEEE Decision and Control Conference, Albuquerque, NM.

8. Mason, M., 1981, "Compliance and Force Control for Computer-Controlled Manipulators," IEEE Transactions on System, Man, and Cybernetics, Vol. SMC-11, No. 6.

9. Raibert, M., and Craig, J., 1981, "Hybrid Position/Force Control of Manipulators," ASME Journal of Dynamic Systems, Measurement, and Control, Vol. 102.

10. Whitney, D., 1982, "Quasi-Static Assembly of Compliantly Supported Rigid Parts, "ASME Journal of Dynamic Systems, Measurement, and Control, Vol. 104.

11. Mason, M., 1982, "Compliant Motion," in *Robot Motion: Planning and Control*, MIT Press, Cambridge, MA.

12. Loncaric, J., 1985, "Geometrical Analysis of Compliant Mechanisms in Robotics," Ph.D. Thesis, Harvard University.

13. Plücker, J., 1865, "On a New Geometry of Space," Phil Trans. Royal Society of London, Vol. 155.

14. Plücker, J., 1866, "Fundamental Views Regarding Mechanics," Phil. Trans. Royal Society of London, Vol 156.

15. Pigoski, T., and Duffy, J., 1993, "An Inverse Force Analysis of a Planar Two-Spring System," Presented at the 1st Austrian IFToMM Symposium, Seggauberg, Austria, 4-9 July 1993.

16. Griffis, M., and Duffy, J., 1992, "Global Stiffness Modeling of a Class of Simple Compliant Couplings," Accepted for publication by Mechanism and Machine Theory, Pergamon Press.

17. Pigoski, T., Griffis, M., and Duffy, J., 1992, "Stiffness Mappings Employing Different Frames of Reference," Flexible Mechanisms, Dynamics, and Analysis, DE-Vol 47, ASME Design Technical Conference 1992. Accepted for publication in the ASME Mechanisms Journal.

18. Loncaric, J., 1987, "Normal Forms of Stiffness and Compliance Matrices," IEEE Journal of Robotics and Automation, Vol RA-3, No. 6.

19. Eijk, J., and Dijksman, J., 1976, "Plate Spring Mechanisms with Constant Negative Stiffness," Vakgroep Fijnmechanische Techniek (Dutch technical report), June.

20. Eijk, J., 1985, "On the Design of Plate Spring Mechanisms," Ph.D. Dissertation, Delft University of Technology, Amsterdam, Holland.

21. Zeeman, E., *Catastrophe Theory: Selected Papers, 1972-1977*, Addison-Wesley Advanced Book Program, Reading, MA, 1977.